Braniewska *et al.*
Cell Communication and Signaling (2024) 22:570
https://doi.org/10.1186/s12964-024-01929-8

Cell Communication and Signaling

RESEARCH

Open Access

A novel process for transcellular hemoglobin transport from macrophages to cancer cells

Agata Braniewska[1,2], Marcin Skorzynski[1], Zuzanna Sas[2,3], Magdalena Dlugolecka[4], Ilona Marszalek[5], Daria Kurpiel[5], Marcel Bühler[7], Damian Strzemecki[5,6], Aneta Magiera[8], Maciej Bialasek[5,9], Jaroslaw Walczak[10], Lukasz Cheda[11], Michal Komorowski[10], Tobias Weiss[7], Małgorzata Czystowska-Kuzmicz[12], Karina Kwapiszewska[8], Alberto Boffi[5,13,14], Magdalena Krol[5,9] and Tomasz P. Rygiel[1,5*]

Abstract

Hemoglobin (Hb) performs its physiological function within the erythrocyte. Extracellular Hb has prooxidative and proinflammatory properties and is therefore sequestered by haptoglobin and bound by the CD163 receptor on macrophages. In the present study, we demonstrate a novel process of Hb uptake by macrophages independent of haptoglobin and CD163. Unexpectedly, macrophages do not degrade the entire Hb, but instead transfer it to neighboring cells. We have shown that the phenomenon of Hb transfer from macrophages to other cells is mainly mediated by extracellular vesicles. In contrast to the canonical Hb degradation pathway by macrophages, Hb transfer has not been reported before. In addition, we have used the process of Hb transfer in anticancer therapy, where macrophages are loaded with a Hb-anticancer drug conjugate and act as cellular drug carriers. Both mouse and human macrophages loaded with Hb-monomethyl auristatin E (MMAE) effectively killed cancer cells when co-cultured in vitro.

Keywords Hemoglobin, Macrophages, CD163, Extracellular vesicles, Monomethyl auristatin E

*Correspondence:
Tomasz P. Rygiel
trygiel@imdik.pan.pl
[1] Department of Immunology, Mossakowski Medical Research Institute, Polish Academy of Sciences, 02-106 Warsaw, Poland
[2] Department of Immunology, Medical University of Warsaw, Warsaw, Poland
[3] School of Molecular Medicine, Medical University of Warsaw, Warsaw, Poland
[4] Chair and Department of Biochemistry, Doctoral School, Medical University of Warsaw, Warsaw, Poland
[5] Cellis AG, Zurich, Switzerland
[6] Department of Experimental Pharmacology, Mossakowski Medical Research Institute, Polish Academy of Sciences, Warsaw, Poland
[7] Laboratory of Molecular Neuro-Oncology, Department of Neurology, Clinical Neuroscience Center, University Hospital and University of Zurich, Zurich, Switzerland
[8] Institute of Physical Chemistry, Polish Academy of Sciences, Warsaw, Poland
[9] Center of Cellular Immunotherapies, Warsaw University of Life Sciences, Warsaw, Poland
[10] Institute of Fundamental Technological Research, Polish Academy of Sciences, Warsaw, Poland
[11] Faculty of Chemistry, University of Warsaw, Warsaw, Poland
[12] Chair and Department of Biochemistry, Medical University of Warsaw, Warsaw, Poland
[13] Department of Biochemical Sciences "Alessandro Rossi Fanelli", Sapienza University of Rome, Rome, Italy
[14] Center of Life Nano and Neuro Science, Italian Institute of Technology, Rome, Italy

Introduction

The effectiveness of cancer treatment is still inadequate, making cancer the number one cause of death in developed countries. Current cancer treatments include surgery, radiotherapy, chemotherapy, or a combination of these three. Conventional chemotherapy is only partially effective, mainly due to a lack of selectivity. Less than 0.1% of the administered chemotherapeutic agent reaches the tumor tissue, while the majority remains in healthy tissue, causing side effects [1]. Therefore, there is an urgent need to develop more effective drug delivery systems to overcome the challenges associated with chemotherapy. In recent years, a variety of nanocarriers have been investigated to improve therapeutic efficacy. Among others, liposomes, nanopolymers, and inorganic nanoparticles have been extensively studied to provide advantages such as controlled release, better targeting, and increased bioavailability of drugs [2]. In addition, live cells such as lymphocytes, monocytes, macrophages, dendritic cells, and erythrocytes have emerged as drug carriers due to their specific properties such as biocompatibility, stability in circulation, natural tissue targeting, and ability to cross biological barriers [3].

Macrophages are the most flexible and diverse cells found in all body compartments, with tissue-specific characteristics and functions. In response to environmental factors, macrophages alter their gene expression profiles, followed by a change of phenotype, metabolism, and activity, known as polarization. The simplest division includes polarization into M1 (proinflammatory) and M2 (anti-inflammatory) macrophages, which represent the extremes of the phenotype continuum. Macrophages present in the tumor microenvironment usually exhibit pro-tumor activity and correlate with poor prognosis. Macrophages are equipped with a variety of receptors (e.g. scavenger receptors, receptors that sense pathogen- and damage-associated molecular patterns) and possess many capabilities, such as chemotaxis, phagocytic activity, the ability to present antigens, the production of oxygen and nitrogen radicals, and release of a plethora of cytokines [4–6]. Macrophages play an essential role in innate immunity, maintaining homeostasis and supporting tissue integrity and functionality. Macrophages are involved in the metabolism of many substances including hemoglobin (Hb), as they support Hb biogenesis and are directly responsible for Hb degradation [7].

Hb is the most abundant protein in the blood. Hb is a tetramer made up of two α and two β subunits. Each subunit consists of globin with an iron-containing heme molecule. The function of Hb is fundamental as it carries oxygen to the tissues [8–10]. In the circulation, free Hb and particularly heme are toxic due to NO scavenging and direct pro-oxidative and proinflammatory reactions, leading to gastrointestinal, cardiovascular, pulmonary, urogenital, hematological, and renal abnormalities [11, 12]. Physiologically, Hb is sequestered in red blood cells, but hemoglobin can be released during hemolysis. To prevent the harmful effects of free Hb, there are several scavengers and mechanisms that ensure Hb detoxification, such as haptoglobin (Hp), hemopexin, CD163, and heme oxygenase. The first step in the canonical pathway of free Hb clearance depends on the formation of the Hb-Hp complex and its further uptake by the CD163 receptor on monocytes/macrophages. However, studies in the mouse model have shown that, in contrast to humans, the formation of Hb-Hp complex does not increase the affinity for CD163 and that CD163 is not required for Hb uptake [13]. Following endocytosis, Hb is degraded in macrophages and converted to end products: amino acids, iron, CO, and bilirubin [14–17].

In the present study, we show that in humans macrophages may uptake Hb independently of Hp and CD163. In addition, we describe a novel pathway of Hb processing by macrophages in which Hb is transferred to the neighboring cells instead of being degraded. This transfer is largely mediated by macrophage-derived extracellular vesicles. The observed phenomenon of Hb transfer can be exploited as a new cellular anticancer conjugate delivery to cancer cells in a new cell-based anticancer therapy. Here, we demonstrate a beneficial therapeutic effect of conjugated Hb to the anticancer drug monomethyl auristatin E (MMAE) in several in vitro cancer cell culture models.

Materials and methods

Cell lines and primary cell culture

Human acute monocytic leukemic cell line THP-1 (ATCC® TIB-202™) was cultured in RPMI-1640 medium supplemented with 10% bovine calf serum (FBS) (VWR), 1% penicillin/streptomycin and 0.05 mM of 2-mercaptoethanol. Murine mammary cancer cell lines EMT6 (ATCC® CRL-2755™) and E0771 (ATCC® CRL-3461™) were cultured in DMEM medium whereas 4T1 (ATCC® CRL-2539™) in RPMI-1640 supplemented with 10% FBS, 1% penicillin/streptomycin and 0.1 mg ml^{-1} Geneticin (Gibco). Human ovarian cancer cell line SKOV-3 (ATCC® HTB-77™), human breast cancer cell line MDA-MB-231 (ATCC® HTB-26™), murine colon cancer cell line CT26.WT (ATCC® CRL-2638™) were cultured in RPMI-1640 medium supplemented with 10% FBS and 1% penicillin/streptomycin. Murine macrophage cell line RAW 264.7 (ATCC® TIB-71™), human colon cancer cell line LoVo (ATCC® CCL-229™), and human cervical cancer cell line HeLa (ATCC® CCL-2™) were cultured in high glucose DMEM medium supplemented with 10% FBS and 1% penicillin/streptomycin. Primary Dermal

Microvascular Endothelial Cells HDMVECs (ATCC® PCS-110–010™), Primary Renal Proximal Tubule Epithelial Cells RPTEC (ATCC® PCS-400–010 ™), Primary Bladder Fibroblast Cells (ATCC® PCS-420–013 ™) were cultured in dedicated media containing all required supplements. MCF10A (ATCC® CRL-10317 ™) epithelial cells were cultured in mammary epithelial basal media (MEBM, Lonza) containing 0.4% bovine pituitary extract (BPE), 10 ng ml^{-1} human epidermal growth factor (hEGF), 5 µg ml^{-1} human insulin, 0.5 µg ml^{-1} hydrocortisone, 30 µg ml^{-1} gentamicin and 15 µg ml^{-1} amphotericin, and 100 ng ml^{-1} cholera toxin (Sigma-Aldrich). Primary human breast fibroblasts were kindly gifted by Monika Puzianowska-Kuźnicka and were cultured in high glucose DMEM medium supplemented with 10% FBS and 1% penicillin/streptomycin. Human Umbilical Vein Endothelial Cells HUVEC (Lonza, C2519A) were cultured in EGM™-2 Endothelial Cell Growth Medium (Lonza). For differentiation to macrophages, THP-1 cells were plated in a medium containing 100 ng ml^{-1} Phorbol 12-myristate 13-acetate (PMA) and incubated for 24 h (37 °C, 5% CO_2) and then for subsequent 24 h in fresh medium w/o PMA.

Peripheral blood mononuclear cells (PBMC) were isolated from buffy coats obtained from blood of anonymous healthy volunteers from the Regional Center of Blood Donation and Treatment in Warsaw with the knowledge of the Bioethics Committee of the Medical University of Warsaw. PBMC were isolated by Lymphoprep™ gradient centrifugation (750 rcf for 30 min, without break). Monocytes were isolated by immunomagnetic positive selection using $CD14^+$ MicroBeads (Miltenyi Biotec) and magnetic separation with QuadroMACS™ Separator (Miltenyi Biotec). Collected cells were seeded in sterile Petri dishes (Ø 100 mm, 1×10^6 cells ml^{-1}) (Promed) and cultured for 7 days (if not stated otherwise) in RPMI-1640 medium supplemented with 10% FBS, 1% Penicillin/Streptomycin and 25 ng ml^{-1} M-CSF (ImmunoTools). On day 5 culture medium was changed to fresh one. For BMDM isolation mice were euthanized, femurs and tibias were isolated. Bones were placed in part of the pipette tip placed in Eppendorf tube and centrifuged (1000 rcf for 1 min). Pellet was resuspended in ACK lysis buffer, incubated for 5 min at RT and passed through 100 µm cell strainer, washed with PBS. Next cells were plated in 5 ml of DMEM:F12 + glutamine/glutamax + 10% FBS + 1% Penicillin/Streptomycin and 20% of L929 conditioned medium and cultured for 7 days (37 °C, 5% CO_2). On day 5 an additional 5 ml of culture medium was added. For M1 or M2 polarization, 6-day old BMDM were stimulated for 48 h using LPS (2 ng ml^{-1}) and IFNγ (50 ng ml^{-1}) or IL-4 (20 ng ml^{-1}) and IL-10 (20 ng ml^{-1}), respectively. List of all key resources with their respective suppliers and reference numbers is included in the Supplemental information (Table S3).

Cell culture procedures

For loading macrophages or PBMC were incubated in Hb (or BSA, haptoglobin when indicated) solution prepared in serum-free medium at concentration 1 mg ml^{-1} of (or other concentration if needed) in constant proportion 10 mln of cells per 1 ml of protein solution for 1 h (37 °C, 5% CO_2) and then washed three times with PBS (Figure S2A). When investigating mechanism of Hb uptake, we preincubated hMDM for 30 min at 37°C with 25 µM 5-[N-ethyl-N-isopropyl] amiloride (EIPA), 4 µM cytochalasin D (cyt D), 20 µM nystatin, 10 µM chlorpromazine (CPZ), 5 mM 2-hydroxypropyl-β-cyclodextrin (HP-β-CD) or 10 ug/ml dextran sulfate, then washed and incubated with Hb-AF488 in serum-free medium for 1 h at 37 °C. Where indicated haptoglobin was mixed with Hb (1:1; w:w), incubated for 10 min at RT and diluted to the concentration needed. For vesicle transfer macrophages were stained with DiD (5 µg ml^{-1} in PBS) for 30 min at 37 °C, washed with PBS and plated in fresh culture medium for 16 h. Cancer cells were stained using CellTrace™ Violet Cell Proliferation Kit or CellTrace™ Far Red Cell Proliferation Kit according to the manufacturer's protocol at working concentration of dye 2.5 µM or 1 µM, respectively. Alternatively, cancer cells were stained using CellTracker™ Orange CMTMR Dye according to manufacturer's protocol at working concentration of dye 5 µM. For flow cytometric analysis or microscopy imaging cells were seeded in ratio 2:1 (macrophages: cancer cells) in RPMI containing 5% FBS and incubated (37 °C, 5% CO_2) for the indicated time with one exception: for co-cultures with macrophages incubated with Hb-MMAE cells were seeded in ratio 1:1. For co-culture without direct contact, 4×10^5 of macrophages were seeded into Transwell® inserts (1 µm pore size) and 2×10^5 of cancer cells were seeded in bottom chamber (Figure S9C). After the indicated time cells were harvested using Trypsin–EDTA solution. For FCS experiments we loaded THP-1 macrophages with mixture of 10 µg ml^{-1} Hb-Alexa Flor 568 and 990 µg ml^{-1} no-labelled Hb (total 1 mg ml^{-1}). Then, 5×10^4 of THP-1 cells and 2.5×10^4 of MDA-MB-231 cells were seeded into µ-Slide 8 Well Glass Bottom chamber slide (ibidi) in 300 µL of RPMI containing 5% FBS. When indicated, co-cultures were performed under shaking (105 rpm). For experiments with conditioned medium, THP-1 macrophages incubated previously with Hb (0.4×10^6) were resuspended in RPMI containing 5% FBS, seeded onto 24-well plate and incubated for 24 h. Cancer cells (0.5×10^5) and standard co-cultures (0.4×10^6 of THP-1 and 0.2×10^6 of cancer cells) were seeded onto 24-well plate and cultured for 24 h. After

that time, medium from above cancer cells was discarded and replaced with medium collected form above macrophages or co-cultures (centrifuged previously at 1000 rcf, 10 min). Cells were cultured for another 24 h and were prepared for flow cytometric analysis. For incubation with EVs, 0.3×10^6 SKOV-3 and MDA-MB-231 cells were seeded onto a 24-well plate and cultured for 24 h. Then, the medium was replaced with fresh medium, mixed with the EVs fraction in a 1:1 volume ratio, and then cultured for another 24 h. After this time, cells were prepared for flow cytometric analysis. For radioactivity measurements, solutions containing radioiodine labelled protein with a concentration of Hb or a mixture of Hb/Hp (1:1; w:w): 1000 μg ml^{-1}, 100 μg ml^{-1}, 10 μg ml^{-1}, 1 μg ml^{-1} were prepared. The concentration of protein was measured at NanoDrop One UV–Vis spectrometer. Radioactive concentration was determined at WIZARD2 2480 Automatic Gamma Counter (PerkinElmer). hMDM were incubated in protein solutions for 1 h (37 °C, 5% CO_2) and washed twice with PBS. Radioactivity of bounded protein was measured at WIZARD2 2480. For cytotoxicity assays hMDM were incubated for 1 h (37 °C, 5% CO_2) in Hb-MMAE solution (100 μg ml^{-1}) prepared in serum-free medium (RPMI-1640) at cell density 10 mln of hMDM per 1 ml, next cells were washed three times with PBS. For other macrophages concentration of Hb-MMAE was indicated in the figure legends. Cancer cells (e.g. MDA-MB-231 or SKOV-3) were seeded on 24-well adherent plate in ratio 8:1, 4:1, 2:1, 1:1 or 1:2 (cancer cells: hMDM) in RPMI-1640 containing 5% FBS, 1% Penicillin/Streptomycin and 25 ng/ml^{-1} M-CSF (ImmunoTools) and incubated for 48–72 h (37 °C, 5% CO_2). Cancer cell monocultures were seeded as control. After incubation cells were harvested using a Trypsin/EDTA solution (Thermo Fisher) and stained for viability using Zombie Aqua (1:600) (BioLegend) and to identify the hMDM population using CD14 antibody. Stained cells were suspended in 200 μl Facs Flow solution. Directly before flow cytometry on FACSCanto II (BD), counting beads (CountBright™, Invitrogen) were added to each sample. The analysis was performed using FlowJo software.

Protein conjugation and radiolabeling

For conjugation reactions proteins were dissolved in 0.1 M $NaHCO_3$ pH 8.3 or in PBS pH 7.4 reaching a final concentration of less than 1 mM. Alexa Fluor NHS Esters were dissolved in DMSO and then diluted in 0.1 M $NaHCO_3$ pH 8.3. Both solutions were mixed in volume ratio 1:1 (when protein was in $NaHCO_3$) or 1:10 (when protein was in PBS) and with fluorochrome to protein molar ratio 2.5:1, incubated for 45–60 min at RT with rotation and then washed and concentrated using Amicon® Ultra-15 Centrifugal Filter Unit with 10 kDa cutoff against 0.1 M $NaHCO_3$ pH 8.3 or PBS pH 7.4. Alternatively, Hb was dissolved in buffer (25 mM HEPES, 10 mM $(NH_4)SO_4$, 10 mM methionine and 0.1 mM EDTA). Alexa Fluor 568 C5 Maleimide was dissolved in DMSO, added to Hb at 5× molar excess, incubated for 3 h at 4 °C and then washed and concentrated using Amicon® Ultra-15 Centrifugal Filter Unit with 10 kDa cutoff against 0.1 M $NaHCO_3$ pH 8.3. Unless otherwise noted, Hb was powdered human hemoglobin, primarily metHb (Lee Biosolutions, #338–10). Alternatively, freshly isolated human or mouse hemoglobin was used. Hb concentration was calculated based on Beer–Lambert law and heme extinction coefficient (167,000 M^{-1} cm^{-1}) at 405 nm for powdered Hb and at 415 nm for fresh Hb. BSA and HSA concentration was measured at NanoDrop spectrophotometer using a protein module.

Conjugation of hemoglobin with MMAE was carried out with a fivefold excess of drug over protein. MMAE derivative with a cleavable dipeptide, valine-citrulline was purchased from MedChemExpress with a declared purity of over 99.90% in the form of a powder and dissolved in a dimethylacetamide solution before the reaction. The conjugation reaction was conducted in buffer containing 20 mM Hepes, 1 mM EDTA, 0.04% Tween 20, pH 7.3 for 2 h at 4 °C. Then, the reaction mixture was washed and concentrated using Amicon® Ultra-15 Centrifugal Filter Unit with 10 kDa cutoff against 0.1 M $NaHCO_3$, 0.02% Tween 20, pH 8.0 (formulation buffer). Reagents for the conjugation reaction were purchased from Sigma Aldrich. The conjugation reaction was confirmed by mass spectrometry, and conjugation efficiency was determined by UV–Vis spectrophotometry using experimentally determined extinction coefficients. The mass spectra were recorded by ESI-QTOF mass spectrometer (Premier, Waters). Samples prepared in a formulation buffer in a concentration of 1 mg ml^{-1} were directly injected into the mass spectrometer. UV–Vis spectra were recorded by DeNovix DS-11 FX + spectrophotometer. The maximum absorbance for hemoglobin was at 405 nm and for the vcMMAE drug was at 252 nm. Experimentally determined extinction coefficient for vcMMAE was 13,642 M^{-1} cm^{-1} at 252 nm and 2 M^{-1} cm^{-1} at 405 nm, and for hemoglobin: 82,887 M^{-1} cm^{-1} at 405 nm and 21,716 M^{-1} $cm^{-}1$ at 252 nm.

For radiolabeling of hemoglobin, 500 μL of $[^{131}I]$ NaI solution (Polatom, Otwock, Poland) was mixed with hemoglobin solution in PBS up to concentration of protein 1 mg ml^{-1}. The sample was transferred into Pierce Pre-Coated Iodination Tubes. Radioactivity of reaction mixture was measured at Atomlab 500 dose calibrator (Biodex Medical Systems), concentration of protein was measured at NanoDrop One UV–Vis

spectrophotometer, then incubated for 120 min in room temperature. Raw product was transferred to Vivaspin 10 k centrifugal filters and washed twice with PBS solution. Radioactivity and concentration of protein were measured as described. The purity of the final product was determined by thin layer chromatography (TLC) and was higher than 92%.

Fluorescence correlation spectroscopy

Fluorescence correlation spectroscopy (FCS) measurements were performed using Nikon Eclipse TE2000U confocal microscope combined with the FCS PicoHarp 300 set. The measurements were carried out in an Okolab climate chamber at 36 °C. Fluorescence was induced by 561 nm pulse laser. Observations were carried out using a 60 × lens (N.A. 1.2) with water immersion. Each measurement was preceded by calibration in a suitable reference medium [18]. The diffusion coefficient of Hb-Alexa Fluor 568 was measured in solutions: serum-free RPMI and $NaHCO_3$. The viscosity of serum-free RPMI and $NaHCO_3$ was estimated based on a comparison of the diffusion coefficient of rhodamine B in water. Hydrodynamic radii of the monomer, dimer, and tetramer of Hb-Alexa Fluor 568 were calculated using the Stokes-Sutherland-Einstein equation, based on the measured diffusion coefficients. The radius of tetramer was calculated based on the diffusion coefficient of Hb-Alexa Fluor 568 in serum-free RPMI, radius of dimer was calculated based on the diffusion coefficient of Hb-Alexa Fluor 568 solution in 0.1 M $NaHCO_3$ pH 8, and radius of monomer was calculated based on the diffusion coefficient of Hb-Alexa Fluor 568 solution in 0.1 M $NaHCO_3$ pH 8. The viscosity of MDA-MB-231 cytoplasm was estimated by using TRITC-labelled dextrans according to the procedure described earlier [19]. Predicted diffusion coefficients of monomer, dimer, and tetramer of Hb-Alexa Fluor 568 in the cytoplasm of MDA-MB-231 were calculated based on the model expressed by a formula [18, 20]:

$$\eta_{\text{eff}} = \eta_0 A \exp\left[\left(\frac{\xi^2}{{R_H}^2} + \frac{\xi^2}{{r_p}^2}\right)^{-a/2}\right]$$

Where:
η_{eff} – effective viscosity of cytoplasm;
η_0 – viscosity of water;
A – factor of the order of 1;
ξ – characteristic length-scale;
R_H – characteristic length-scale;
a – exponent indicating type of complex fluid;
r_p – hydrodynamic radius of a probe.

The model was previously validated for MDA-MB-231 cells [21] with the following parameters: $A = 1.3 \pm 0.3$, $\xi = 1.70 \pm 0.29$ nm, $R_H = 2.85 \pm 0.92$ nm, $a = 0.55 \pm 0.15$.

FCS analysis in the cytoplasm of MDA-MB-231 cells was performed after 4 and 6 h of co-culture with Hb-Alexa Fluor 568-loaded THP-1 macrophages. FCS autocorrelation curves obtained for Hb-Alexa Fluor 568 is MDA-MB-231 cytoplasm were fitted by a two-component normal diffusion model.

EV separation and labeling

First, the medium was centrifuged at 2000 rcf for 10 min at RT, the supernatant was centrifuged again at 10,000 rcf for 30 min at 4 °C. Finally, the sample was filtered using a 0.22 µm PVDF syringe filter (Merc), and directly used for EV-isolation. The homemade mini-SEC columns were prepared as described by Ludwig et al. using Sepharose CL-2B [22, 23]. A 1 ml of precleared medium was applied to the mini-SEC column. After the sample entered the column, 2 ml of PBS was added, and 3 ml of void volume was collected (fractions 1–3, 1 ml each). Then, 4 ml of PBS was added, and EV-enriched fractions (4, 5 and 6; 1 ml each) were collected in separate tubes. For membrane labeling of EVs, the lipophilic membrane dye CellMask™ Plasma Membrane was used at a final concentration of 4 ng ml^{-1} as described before [23]. Briefly, prediluted EVs and prediluted in the dye solution at 9:1 ratio in a total volume of 10–50 µl were incubated for 2 h at RT in the dark. Then, the EVs were further diluted in PBS (usually 1:1000) and measured by Nanoparticle Tracking Analysis (NTA) at RT at 11 positions in one cycle with the following settings: F640, Sensitivity: 91, Shutter: 100, Minimal Brightness: 25, Trace length: 7, Min Area: 10, Max Area: 1000 nm/Class: 5, Classes/Decade: 64, Resolution: medium. All labelled samples were first evaluated in fluorescence mode with the function "low bleach" on, immediately followed by evaluation in scatter mode to minimize photobleaching. At least three measurements of each sample were performed.

EV analysis

EV size distribution and concentration were obtained using the ZetaView PMX220 instrument (Particle Metrix, Germany) equipped with a 488 and 640 nm laser and ZetaView 8.05.11 SP4 software. The measurement was performed as described before [23]. Briefly, the measurements in scatter mode were performed at 25 °C at 11 positions in two cycles with the following settings —Sensitivity: 80, Shutter: 100, Minimal Brightness: 30, Trace length: 15, Min Area: 10, Max Area: 1000 nm/Class: 5, Classes/Decade: 64, Resolution: medium. The camera sensitivity was adjusted to also detect dim particles at a minimal background noise (measured in PBS).

All settings were kept the same for all analyzed samples to minimize variability. At least three measurements of each sample were performed. EVs were measured in F488 mode using the following settings: F488, Sensitivity: 95, Shutter: 100, Minimal Brightness: 25, Trace length: 7, Min Area: 10, Max Area: 1000 nm/Class: 5, Classes/Decade: 64, Resolution: medium.

A concentrated EV sample consisting of SEC fractions 4–6 from sample THP-1 Hb-AF488 (10 µg) was incubated with mix of Dynabeads: Exosome-Human CD69/CD9/CD81 Flow Detection Reagents (Thermo Fisher Scientific 10606D, 10620D, 10622D) following the manufacturer's protocol. Briefly, the EV sample volume was adjusted to 100 µl using isolation buffer (PBS with 0.1% BSA, filtered through a 0.22 µm filter). Then, 20 µl of Dynabeads were washed with isolation buffer and added to the EV sample. The sample was incubated ON with shaking (600 rpm) at 4 °C. The following day, the Dynabead-bound EVs were stained with the tetraspanin markers (CD63-PE, CD9-FITC, CD81-APC) or the isotype controls for 1 h at RT with mild shaking (600 RPM), then washed with isolation buffer and analyzed by flow cytometry. Flow cytometry was performed on a BD FACSVerse 8 Color Flow Cytometer (BD) with BD FACSuite Software v.1.0.6. FCS files were then analyzed with FlowJo Software. The stained bead-coupled EVs were resuspended in 150 µL PBS. A single-bead gate was set based on the FCS and SSC scatter and a minimum of 1500 beads were acquired.

Proteomics measurements

Sample processing: EV samples were dried in a Speedvac to remove the remaining buffer and resuspended in 10 µl lysis buffer (8 M urea in 100 mM Tris/HCl pH 8.2). Samples were sonicated by high-intensity focused ultrasound (UP200St, Hielscher Ultrasonics GmbH) for 3 × 20 s at 60% amplitude, reduced with 1 µl of 100 mM tris(2-carboxylethyl)phosphin for 30 min at 37 °C/600 rpm and alkylated with 1 µl of 200 mM chloroacetamide under light protection for 30 min at 25 °C/600 rpm in a thermomixer. Lysis buffer was diluted by adding 55 µl of a 50 mM triethylammonium bicarbonate (pH 8.5) followed by digestion with 100 ng trypsin (Promega) for 16 h at 37 °C/600 rpm in a thermomixer. Digestion was stopped with 20 µl of 10% formic acid. Data acquisition and quantification: Peptides corresponding to 450 µg protein input were spiked with iRT peptides (Biognosys) and loaded onto Evotips (Evosep Biosystems). Peptides were separated with an Evosep One chromatography system (Evosep Biosystems) equipped with a PSC-15–100-3UHPnC ReproSil C18 3 M PepSep analytical column (15 cm length, 120 Å pore size, 100 µm inner diameter). The system was operated at the 30 samples per day (30 SPD) setting (44 min gradient) with a flow rate of 0.5 µl min^{-1}. Peptides were analyzed on-line by a timsTOF Pro mass spectrometer (Bruker Daltonics) using the standard 1.9 s cycle time dda-PASEF acquisition mode. Precursor mass range was set to 100–1700 m/z and the inverse mobility range (1/k0) was set between 0.6–1.6 cm^2 V^{-1} s^{-1} with a mobility-dependent collision energy of 20 eV at 0.85 cm^2 V^{-1} s^{-1} and 59 eV at 1.3 cm^2 V^{-1} s^{-1}. Raw data was searched against a human Uniprot database (2022–06-16-decoys-reviewed-contam-UP000005640.fas, 2,810,144 peptides) containing decoy sequences and common contaminants and quantified with Fragpipe/MSFragger (v3.4) [24] using IonQuant (v1.7.17) and Philosopher (v4.5.1) at standard settings. Carbamidomethylation of cysteines was set as fixed modification whereas methionine oxidation and N-terminal acetylation were set as variable modifications. Data analysis: The "combined_protein" table was imported into R/RStudio, normalized by median absolute deviation (MAD) normalization based on the MaxLFQ intensities, followed by removal of non-human contaminants and filtering for proteins detected in at least 2/3 of control samples (766 proteins, 12.6% missingness). Missing data was imputed based on a mixed imputation approach (maximum likelihood estimation/MLE for missing completely at random/MNAR data; imputation under a Gaussian complete data assumption/IGCDA for missing not at random/MNAR data) using the 'imp4p' package [25]. Batch correction and differential expression were performed using the 'limma' package [26]. Identification of cell surface proteins was performed as described in the main text using a Uniprot reference list based on the Uniprot keywords 'cell membrane' (KW1003), 'membrane' (KW0472) and 'secreted' (KW0964). Pathway overrepresentation analysis (ORA) was performed with the 'WebgestaltR' package (https://github.com/bzhanglab/WebGestaltR) using the cell surface protein list extracted from Uniprot as background. GO Biological Processes, Cellular Components and Molecular Function (non-redundant pathways) as well as pathways from the Kyoto Encyclopedia of Genes and Genomes (KEGG) and the Reactome database were included in the analysis. Heatmaps were generated using the ComplexHeatmaps package [27]. Among the detected surface proteins, most distinctive proteins between Hb-treated and control conditions were identified using a two-group linear discriminant analysis (LDA), as implemented in the LDA function of the 'MASS' package (http://www.stats.ox.ac.uk/pub/MASS4). Top hits were identified based on LD1 weight

scores (LD1 > 0.045 or LD1 < -0.025) and assessed by individual Student's t-test.

Statistics

Data is presented as mean ± SD. Statistical analysis was performed with GraphPad Prism10 software using a paired or unpaired 2-tailed Student's t-test or one-way ANOVA. *P* values less than 0.05 were considered statistically significant. Except for proteomic analysis, the statistical details of experiments can be found in the figure legends, statistical details of the proteomic analysis are described in the appropriate section of the Methods.

Results

Macrophages take up Hb independently of CD163

To prevent harmful effects, free Hb is taken up and detoxified by monocytes and macrophages [14]. Flow cytometric analysis showed that among peripheral blood mononuclear cells, only monocytes were able to take up free Hb, whereas B cells, NK cells, NKT cells, and T cells did not take up Hb (Fig. 1A), which is consistent with the function of monocytes as intravenous Hb scavengers [28]. To investigate Hb uptake by macrophages, we used human and murine primary macrophages (human monocyte-derived macrophages (hMDM), murine bone marrow-derived macrophages (BMDM)) and cell lines including PMA-differentiated THP-1 cells and RAW 264.7 cells. All studied macrophages were able to take up human Hb during 1-h incubation as we showed by flow cytometry (Fig. 1B) and confocal microscopy (Figure S1A). Additionally, using a panel of macrophages this process was confirmed by Western blot (Figure S1B). To evaluate the kinetics of the Hb uptake, we incubated THP-1 macrophages with Hb for 5–120 min and examined cell fluorescence at several time points. Hb uptake was very fast, Hb was present in cells already after 5 min and increased over time (Figure S1C).

Although previous studies suggested that the main route of Hb uptake is via CD163 [15, 29, 30], later reports in the murine model indicated that CD163 is not required for this process [13]. We observed that CD163 is not required for Hb uptake by macrophages, as some macrophages (RAW 264.7 and BMDM) do not express CD163 mRNA (Figure S1D), but still took up Hb from the medium. Among the studied macrophages, hMDM had the highest expression of CD163 mRNA, but only 2.3–9.7% of hMDM expressed CD163 protein on the cell surface, and the percentage of $CD163^+$ hMDM varied between donors (Figure S1E). We next incubated hMDM with two concentrations of Hb (0.01 mg ml^{-1} and 1 mg ml^{-1}) and then stained the cells with CD163 antibody. We found that both $CD163^+$ and $CD163^-$ populations of hMDM were able to uptake Hb (Fig. 1C, Figure S1F), demonstrating that the CD163 receptor is not required for Hb uptake by macrophages. $CD163^+$ cells had a higher mean fluorescence intensity (MFI) than the $CD163^-$ population (Fig. 1D, Figure S1G), suggesting that $CD163^+$ cells took up Hb more efficiently, but due to the $CD163^+$ frequency, the MFI of the total cell population was similar to $CD163^-$ subpopulation (Fig. 1D, Figure S1G). We further investigated the importance of haptoglobin, which can form a complex with free Hb and binds to CD163. To this end, we evaluated the uptake of Hb/Hp complexes [30]. We observed that the presence of Hp did not increase Hb uptake by hMDM at the four concentrations of Hb (Fig. 1E). We then examined the uptake of Hb or Hb/Hp by $CD163^+$ and $CD163^-$ hMDM. The presence of Hp increased Hb uptake only in $CD163^-$ hMDM at the higher Hb concentration (1 mg ml^{-1}). In general, $CD163^+$ hMDM took up more Hb, but the presence of Hp did not affect the efficiency of Hb uptake (Fig. 1F). In contrast to all previous experiments, where we incubated macrophages with Hb in a serum-free medium, the addition of human serum (20%) to the medium, as a potential source of haptoglobin, did not significantly change neither the percentage of Hb-positive macrophages nor the fluorescence intensity of Hb in macrophages (Figure S1H-I). To investigate the mechanism of Hb uptake we used inhibitors of several cellular uptake mechanisms including 5-[N-ethyl-N-isopropyl] amiloride (EIPA,

(See figure on next page.)

Fig. 1 Macrophages uptake Hb independently of CD163. **A** Mean fluorescence of Hb in the population of PBMC. Human PBMC were incubated with 0.1 mg ml^{-1} Hb-AF488 for 1 h, stained with monoclonal antibodies (a-CD14, a-CD3, a-CD56, a-CD19) and analyzed by flow cytometry. Data from 10 donors. **B** Human monocyte-derived macrophages (hMDM), PMA-differentiated THP-1 cells, murine bone marrow-derived macrophages (mBMDM) and RAW 264.7 cells were incubated with 0.2 mg ml^{-1} Hb-AF488 for 1 h and analyzed by flow cytometry. C-D. Flow cytometric analysis of hMDM after 1-h incubation with Hb-AF488 and staining with a-CD163 antibody. Representative graphs (**C**.) and mean fluorescence of Hb in hMDM (**D**.). Data from 3–5 donors. **E** Percentage of ^{131}I-Hb taken up by hMDM after 1-h incubation with indicated concertation of Hb or Hb/Hp. *$P < 0.05$. **F** Mean fluorescence of Hb in hMDM. Cells were incubated with Hb-AF488 or Hb-AF488/Hp for 1 h, stained with a-CD163 antibody and analyzed by flow cytometry. Data from 3–5 donors. **$P < 0.01$. G-H. Mean fluorescence of Hb in hMDM preincubated for 30 min with inhibitors (25 µM 5-[N-ethyl-N-isopropyl] amiloride (EIPA), 4 µM cytochalasin **D** (cyt D), 20 µM nystatin, 10 µM chlorpromazine (CPZ), 5 m M 2-hydroxypropyl-β-cyclodextrin (HP-β-CD) or 10 ug ml^{-1} dextran sulfate) and then incubated for 1 h with 0.01 (**G**.) or 1 mg ml^{-1} (**H**.) Hb-AF488. $n = 5$ donors. *$P < 0.05$, ** $P < 0.01$, ***$P < 0.001$, ****$P < 0.0001$. Data are presented as the mean ± SD

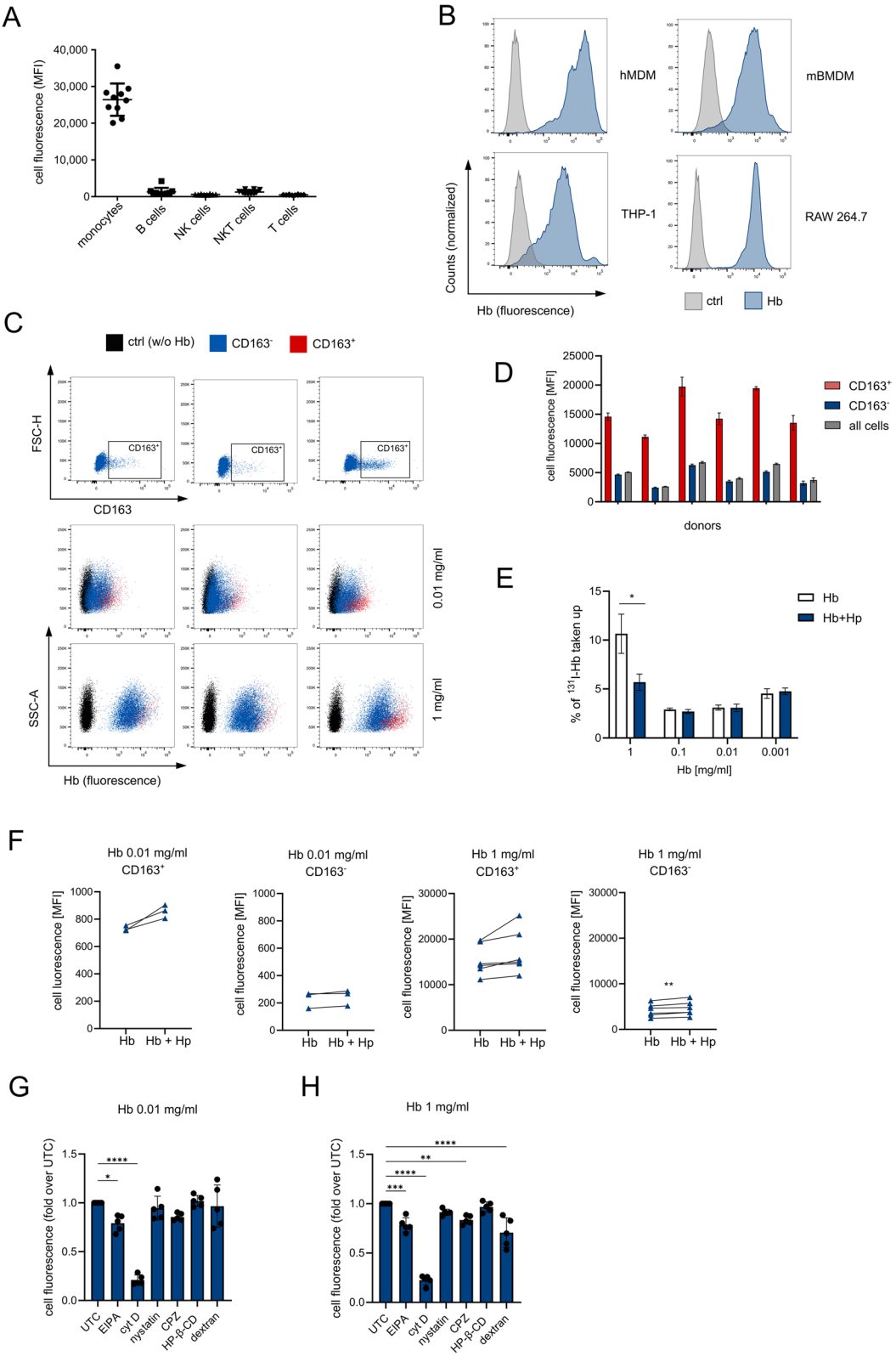

Fig. 1 (See legend on previous page.)

inhibitor of micropinocytosis), cytochalasin D (cyt D, inhibitor of actin polimeryzation), nystatin (inhibitor of the caveolae-mediated endocytosis), chlorpromazine (CPZ, inhibitor of the clathrin-mediated endocytosis), 2-hydroxypropyl-β-cyclodextrin (HP-β-CD, inhibitor of the lipid raft-mediated endocytosis) and dextran sulfate (a competitive inhibitor for scavenger receptor). EIPA and cyt D decreased uptake of lower dose of Hb (10 μg ml^{-1}) and EIPA, cyt D, chlorpromazine and dextran inhibited uptake of higher dose of (1 mg ml^{-1}) (Fig. 1G-H) suggesting that multiple mechanisms are involved in Hb uptake of macrophages. Taken together, these results indicate that Hb can be taken up by macrophages independently of Hp or CD163.

Macrophages transfer Hb to neighboring cells

The canonical understanding is that macrophages take up free Hb and degrade it to prevent the toxic effects of free Hb and in particular heme [14, 16]. Interestingly, we observed that a certain amount of Hb was transferred to the neighboring cells. We incubated THP-1 macrophages with 1 mg ml^{-1} fluorescently labelled-Hb and then co-cultured them with four fluorescently labelled cancer cell lines: HeLa, MDA-MB-231, SKOV-3, and LoVo (Figure S2A-B). Using flow cytometry, we distinguished the cancer cell populations from the macrophages and measured the fluorescence of Hb according to the gating strategy shown in Figure S3. After 24 h of co-culture, we observed a clear fluorescence signal of Hb in cancer cells (Fig. 2A-C). The cell–cell transfer of Hb was very efficient, reaching up to 90% of Hb-positive cancer cells over the monitored period (Fig. 2B). Based on the mean fluorescence (MFI) of Hb in cancer cells, we concluded that the efficiency of Hb transfer varied in different cell lines, with the highest transfer observed in SKOV-3 cells (Fig. 2C). We confirmed the transfer of Hb to cancer cells by microscopy, as we observed fluorescent signals from Hb inside cancer cells after co-culture with Hb-preincubated THP-1 macrophages (Fig. 2D). In addition to THP-1 macrophages, hMDM, BMDM and RAW264.7 cells also transferred Hb to cancer cells (Figure S4A-C). To evaluate the dynamics of Hb transfer, we analyzed cells from co-cultures performed for 2–48 h. Hb transfer from THP-1 macrophages to SKOV-3 cells was time-dependent and increased gradually, starting from 8% Hb^+ cancer cells after 2 h, up to 40–45% Hb^+ cells after 24–48 h (Fig. 2E). The efficiency of Hb transfer, expressed as cancer cell fluorescence after co-culture, was dependent on the Hb concentration during macrophage loading, as the higher the Hb concentration, the higher the cancer cell fluorescence (Fig. 2F). The efficiency of Hb transfer increased with increasing cell density in co-culture (Figure S4D).

To test the importance of the source of Hb we have compared 3 forms of Hb: fleshly isolated mouse and human Hb together with powdered form of human Hb used in the previous experiments. All of them were taken up by BMDM and hMDM (Figure S4E). All Hb variants were transferred by macrophages to cancer cells from the respective species, with powdered form of Hb being most efficiently transferred (Fig. 2G). We also investigated the specificity of Hb transfer with respect to recipient cells. We co-cultured Hb-loaded THP-1 macrophages with cancer and non-cancer cells (fibroblasts, epithelial and endothelial cells). We observed a shift in the fluorescence of the recipient cells (Fig. 2H), suggesting that Hb is efficiently transferred to normal cells, particularly epithelial and endothelial cells. Similarly, Hb is transferred between macrophages (Figure S4F), suggesting that this process is not restricted to cancer cells. To test whether the Hb transfer was a unique process, we examined the transfer of other proteins, bovine serum albumin (BSA) and human serum albumin (HSA). Flow cytometric

(See figure on next page.)

Fig. 2 Macrophages transfer Hb to neighboring cells. **A**-**C**. Flow cytometric analysis of cancer cells after 24-h co-culture with THP-1 macrophages incubated previously with Hb-AF488. **A** Representative dot plots that present shift in fluorescence of Hb-AF488 in cancer cells **B** Percentage of Hb-positive cancer cells (HeLa, MDA-MB-231, SKOV-3, LoVo). **C** Mean fluorescence of cancer cells. **D** Representative images of 24-h co-culture of MDA-MB-231 cells and THP-1 macrophages incubated previously with Hb-AF488. Green-Hb-AF488, blue-DAPI (nuclei), red-CellTrace Far Red (cancer cells). Scale bar = 50 μm. **E** Time course of Hb transfer: Percentage of Hb-positive SKOV-3 cells after co-culture with THP-1 macrophages incubated previously with Hb-AF488. Co-culture was conducted for indicated periods. **F** Mean fluorescence of Hb in MDA-MB-231 after 24-h co-culture with THP-1 macrophages incubated previously with different concentrations of Hb-AF488. **G** Percentage of Hb-positive cancer cells (EMT6, SKOV-3) co-cultured with BMDM or hMDM that were incubated previously with freshly isolated mouse and human Hb-AF488 (fresh mHb and fresh hHb respectively) and powdered human Hb-AF488 (hHb). **H** Mean fluorescence of Hb in recipient cells after 24-h co-culture with THP-1 macrophages incubated previously with Hb-AF488. **I** Percentage of Hb- or BSA-positive cancer cells (MDA-MB-231, SKOV-3) after 24-h co-culture with THP-1 macrophages incubated previously with Hb-AF488 or BSA-AF488. **J** Percentage of Hb- or HSA-positive cancer cells (SKOV-3) after 24-h co-culture with hMDM incubated previously with Hb-AF488 or HSA-AF488. ****$P < 0.0001$. A-F, H-I. Experiments were repeated at least 2 times and the representative results are shown. **K** Distribution of average diffusion coefficients for the faster component of Hb-AF568 in the cytoplasm of MDA-MB-231 cells. Predicted diffusion coefficients for various forms of Hb were marked with colored dashed lines. Data are presented as the mean ± SD

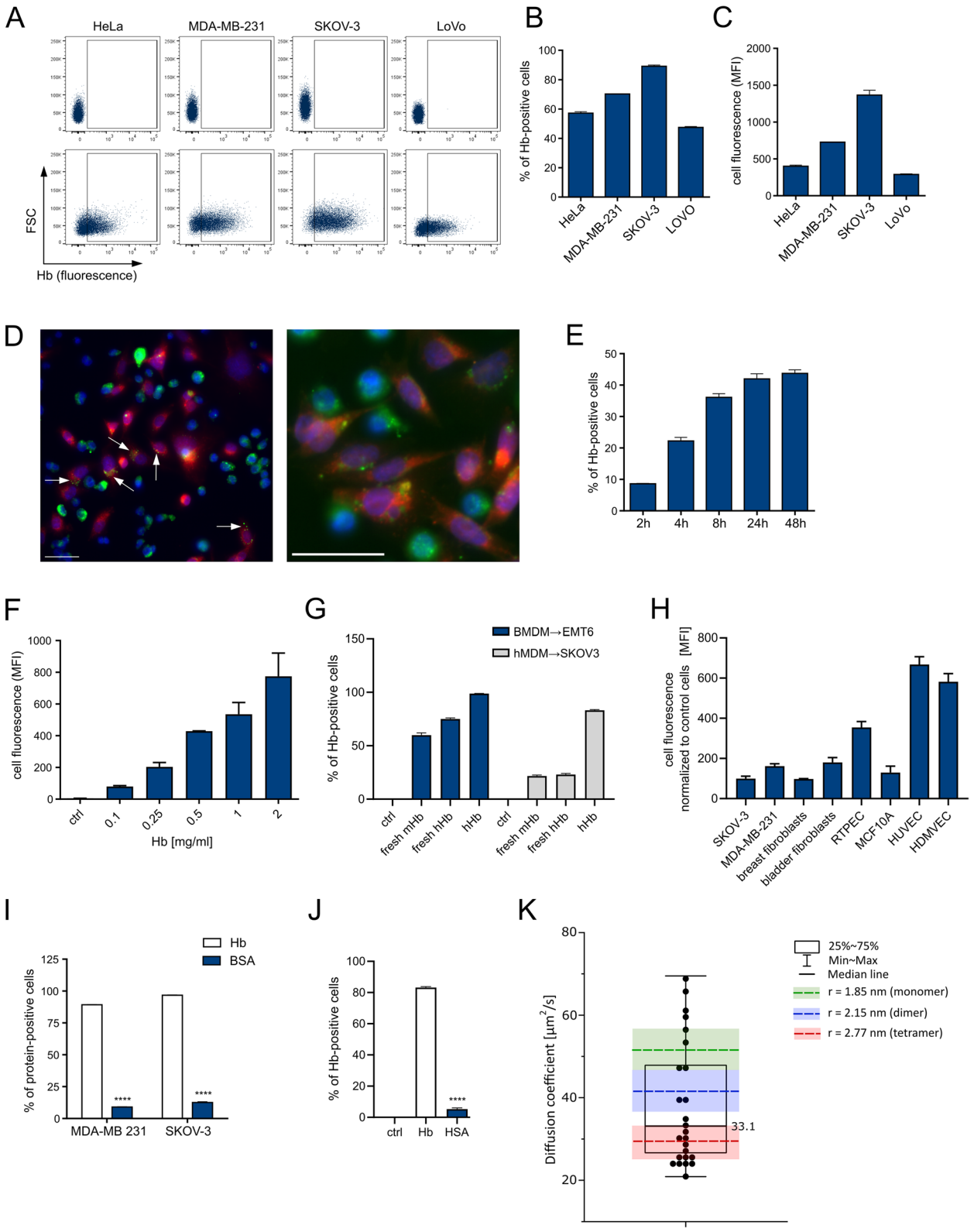

Fig. 2 (See legend on previous page.)

analysis revealed that albumin was taken up by THP-1 macrophages (Figure S5A), RAW264.7 cells (Figure S5B) and hMDM (Figure S5C). In comparison to Hb, BSA or HSA was almost not transferred from these macrophages to cancer cells (Fig. 2I,J Figure S5D-E).

To better understand the phenomenon of Hb transfer and the fate of Hb in cancer cells, we used fluorescence correlation spectroscopy (FCS). FCS is a method that allows studying the cellular uptake of a molecule into a living cell by measuring its diffusion coefficient in the cellular interior. It is based on a cytoplasmic viscosity model for different length scales [18–21]. Utilizing this model and knowing the hydrodynamic radius of the probe, it is possible to predict the diffusion coefficient in the cytoplasm. FCS is sensitive to fluorescence fluctuations of mobile molecules, and the shape of the FCS autocorrelation curve reflects the diffusion regime [18, 31]. By FCS, we determined which form of Hb was present in the cytoplasm of cancer cells after the transfer from macrophages (Figure S6A). Firstly, free Hb-Alexa Fluor 568 was analyzed in solution to measure the hydrodynamic radius of the Hb monomer, dimer, and tetramer. We obtained 1.85 nm, 2.15 nm, and 2.77 nm, respectively (Table S1). These values are similar to those obtained using dynamic light scattering (DLS) for unlabeled Hb oligomers, which are 1.58 nm, 2.11 nm and 2.81 nm, respectively [32]. The predicted diffusion coefficients of these three forms of Hb were calculated based on the length-scale dependent viscosity model [19, 21]. Fluorescence fluctuations were then measured in the cytoplasm of MDA-MB-231 cells after 6 h of co-culture with macrophages preincubated with Hb-Alexa Fluor 568. Examples of the obtained FCS signal and autocorrelation curve with a free diffusion model fit are shown in Figure S6B-C and S6D, respectively. The presence of the free AF568 dye was neglected based on the diffusion coefficients (Fig. 2K, Table S1). The diffusion coefficients of the detected components were heterogeneous and corresponded to monomers, dimers, and tetramers (Fig. 2K). The median value obtained corresponded to the tetramer radius obtained in vitro, suggesting that a tetramer is a predominant form of Hb in the cytoplasm of cancer cells after transfer. We also observed an additional component with a low diffusion coefficient and large variability in the range of 3 $\mu m^2 s^{-1}$ to 0.0001 $\mu m^2 s^{-1}$. These values are characteristic for the diffusion coefficient of small membrane structures and the active transport of endosomes. This suggests the binding of Hb to the membranes of vesicles. In conclusion, Hb is transferred from macrophages to non-cancer and cancer cells mainly in tetrameric form, and this process is protein-selective.

Hb is transferred in extracellular vesicles

To study mechanism of Hb transfer from macrophages, we firstly investigated role of several factors engaged in intracellular trafficking and cell mobility. We observed a decreased percentage of Hb-positive cancer cells when co-culture was conducted in the presence of brefeldin A or monensin (Figure S7A) suggesting the involvement of intracellular protein and vesicular transport machinery in Hb transfer. Inhibition of actin filament polymerization using cytochalasin D (cyt D) or latrunculin B (lat B) almost completely blocked Hb transfer (Figure S7B). In contrast, inhibition of microtubule polymerization using nocodazole (NOCO) reduced the percentage of cancer cells receiving Hb by 41% in MDA-MB-231 cells and by 30% in SKOV-3 cells (Figure S7B). Since actin is involved in many cellular processes, we then investigated selected factors that mediate actin polymerization. Results were not conclusive except of ROCK inhibitors that significantly increased the percentage of Hb-positive cancer cells after co-culture with THP-1 macrophages (Figure S7C). Taken together, the proper function of the actin cytoskeleton is required for the Hb transfer, whereas microtubules play a less crucial role.

One of the mechanisms of intercellular communication in which actin plays an essential role is the formation of tunneling nanotubes (TNT) [33]. Using confocal microscopy we observed TNT-like actin structures, however Hb was rarely present in them (Figure S8A). TNTs are sensitive to mechanical stress, so the formation of TNTs is disrupted by gentle shaking [34, 35]. The efficiency of Hb transfer from THP-1 macrophages to SKOV-3 is not reduced by mechanical stress, however, Hb transfer to MDA-MB-231 cells is slightly reduced under shaking suggesting the importance of TNTs in Hb transfer to these cancer cells (Figure S8B). To better understand the importance of TNTs in the transfer of Hb to MDA-MB-231, we determined the influence of the M-Sec protein on Hb transfer. M-Sec has been described as a regulator of TNT formation in macrophages and cancer cells [36–38]. Downregulation of M-Sec did not significantly affect Hb transfer (Figure S8C-D). The above results suggest that TNTs only contribute to Hb transfer to a minor extent.

We then investigated whether Hb was secreted into the culture media and then taken up by the recipient cells. After incubation with fluorescent Hb for 1 h, THP-1 macrophages were cultured for 24 h, then the medium was collected, centrifuged to remove cells, and transferred to cancer cells for 24 h. Flow cytometric analysis revealed a shift in fluorescence of cancer cells incubated with THP-1 conditioned-medium (Fig. 3A-C), demonstrating that Hb is secreted from THP-1 cells and taken up by cancer cells from the medium. As a control,

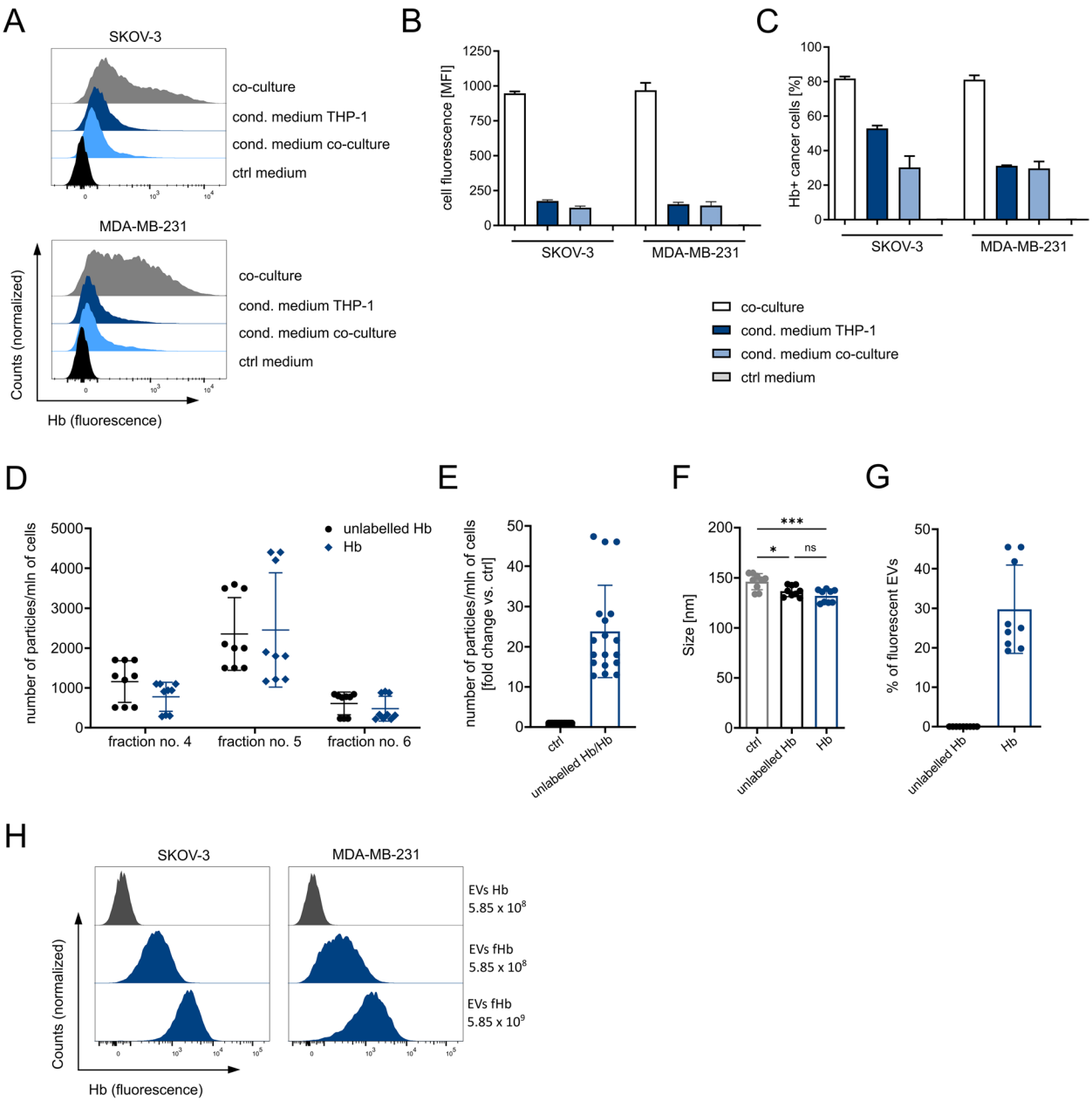

Fig. 3 Hb is transferred in extracellular vesicles **A**-**C**. Flow cytometric analysis of cancer cells after incubation with medium collected from 24-h culture of THP-1 macrophages incubated previously with Hb-AF488, medium collected from 24-h co-culture or control medium. As a control, cancer cells from co-culture were shown. **A** Representative histograms. **B** Mean fluorescence of Hb in cancer cells. **C** Percentage of Hb-positive cancer cells. **D**-**G** NTA analysis of particles isolated from medium collected from THP-1 macrophages incubated previously with Hb or Hb-AF488. D. Number of particles collected in SEC fractions 4–6. E. Number of particles collected in fraction no. 5. F. Size of particles collected in fraction no. 5. *$P < 0.05$, ***$P < 0.001$. **G** Percentage of fluorescent particles in fraction no. 5. **H** Flow cytometric analysis of cancer cells incubated for 24 h with EVs (fraction no. 5) from medium collected from THP-1 macrophages incubated previously with Hb-AF488. Histograms represent the shift in fluorescence of cancer cells. A-C and H. Experiments were repeated at least 2 times and the representative results are shown. D-G. Data pooled from 3 independent experiments. Data are presented as the mean ± SD

fluorescence of cancer cells after co-culture and fluorescence of cancer cells incubated with a medium taken from co-culture were shown. There was no difference in mean fluorescence between cancer cells incubated with a THP-1-conditioned medium and a conditioned medium obtained from THP-1/cancer cell co-culture, indicating that cancer cells are not required for Hb release from THP-1 macrophages.

Hb transfer is less efficient when serum is present in the co-culture media (Figure S9A). In addition, Hb transfer was inhibited when co-cultured cells were separated by a membrane with 1 μm (Figure S9B-C) suggesting a mechanism related to direct cell-to-cell contact. However, such experiments should be interpreted circumspectly since according to literature TNT may penetrate membranes through pores, and on the other hand, the transfer of vesicles can be reduced by 85% [39]. Furthermore, inhibition by a physical membrane indicated that Hb was not transferred as a free protein, but inside larger particles. Therefore, we investigated the role of extracellular vesicles in Hb transfer. First, we co-cultured cancer cells with THP-1 macrophages stained with the lipophilic dye DiD, which is used to track vesicles [40], and observed a shift in fluorescence of cancer cells (Figure S9D), indicating the transfer of vesicles from macrophages to cancer cells.

We then analyzed conditioned medium collected from THP-1 macrophages incubated with unlabelled Hb or fluorescently labelled Hb and then cultured for 24 h. We isolated extracellular vesicles by size-exclusion chromatography (SEC). Nanoparticle Tracking Analysis (NTA) was used to measure the concentration and size of the particles. Particles were observed in fractions 4–6, with the highest concentration in fraction no. 5 (Fig. 3D) and there was no difference in the number of particles produced by cells incubated with unlabelled Hb compared to cells incubated with fluorescently labelled Hb (Fig. 3D). Hb-treated cells released approximately 24 times more particles than control THP-1 macrophages (counted in fraction no. 5) (Fig. 3E). Particles from fraction no. 5 released by THP-1 incubated with unlabelled Hb or Hb had an average size of 137 nm and 132 nm, respectively, and were slightly smaller than particles released by control THP-1 macrophages (average size 143 nm) (Fig. 3F). To verify that the measured particles contained lipids, we stained the fractions with the lipophilic dye Cell Mask Deep Red (CMDR). The size distribution of particles labelled with CMDR was similar to the size distribution measured in scatter mode (Figure S10A). These results suggest the presence of the membrane in the enriched particles. Knowing that the culture medium (without serum) is free of lipoproteins, we concluded that the enriched particles are EVs. Using NTA, we measured that on average 30% of the EVs collected and enriched from fHb loaded THP-1 were fluorescent for AF488 (Fig. 3G). The size distribution measured in scatter mode overlapped with the size distribution measured in fluorescence mode, meaning that fluorescent EVs were similar in size to EVs (Figure S10A). To characterize EVs, we performed bead-based flow cytometry. Using beads, we captured particles expressing classical tetraspanins (CD9, CD81, CD63) and then we stained them with antibodies against CD9, CD81, and CD63. We observed that enriched particles expressed CD9, CD81, and CD63 (Fig S10B), but the fraction of EVs expressing these selected tetraspanins did not contain fHb, as there was no shift in fluorescence (Figure S10C). Finally, we applied the enriched EVs to cancer cells and incubated them for 24 h. Flow cytometric analysis of cancer cells revealed a dose-dependent shift in fluorescence of both SKOV-3 and MDA-MB-231 cells indicating uptake of fluorescent Hb-containing EVs by cancer cells (Fig. 3H).

To characterize the molecular cargo of EVs we performed proteomic analysis of EVs released from cells incubated with Hb and control cells. We found that approximately 45% of all proteins identified were common to EVs released from control and Hb-treated cells. 631 proteins were found exclusively in EVs from Hb-treated cells and 130 proteins were found exclusively in the control EVs (Fig. 4A). Differential expression analysis revealed proteins that are more abundant in EVs released from Hb-loaded cells, one of which is the beta subunit of Hb (Fig. 4B). Proteins upregulated in EVs from Hb-treated cells were evaluated for potential functional insights. Pathway overrepresentation analysis revealed many enriched pathways (Figure S11A) including RNA processing, protein metabolism, cell cycle, chromatin organization, and cell development. To characterize EVs we focused on membrane proteins. The Uniprot database was searched for potential membrane-associated proteins using the Uniprot keywords (cell membrane—KW1003, membrane—KW0472, secreted—KW0964). A total of 858 Uniprot surface proteins were detected in all samples, of which 537 surface proteins were quantified in at least 2/3 of all samples. Approximately half (52.6%; 287 proteins) were detected in both groups, 14.3% (78 proteins) were found only in controls and one-third (33.2%; 181 proteins) were specific for EVs isolated from Hb-treated cells (Figure S11B). To extract proteins that best discriminated between Hb-treated THP-1 macrophages and controls, a simple two-group linear discriminant analysis (LDA) was performed and the top proteins, based on positive/negative weight scores, were selected for hierarchical clustering. Most of the selected proteins showed a significant difference in abundance (Table S2). Next, the cell surface proteins detected only in EVs from Hb-treated THP-1 macrophages were evaluated for potential functional insights (Fig. 4C). Pathway overrepresentation analysis revealed 48 enriched pathways. Many of the over-represented pathways involve various components of vesicular transport and secretory pathways, including COPI-dependent transport. This suggests that macrophages secrete different types of EVs upon loading with Hb, with vesicle composition

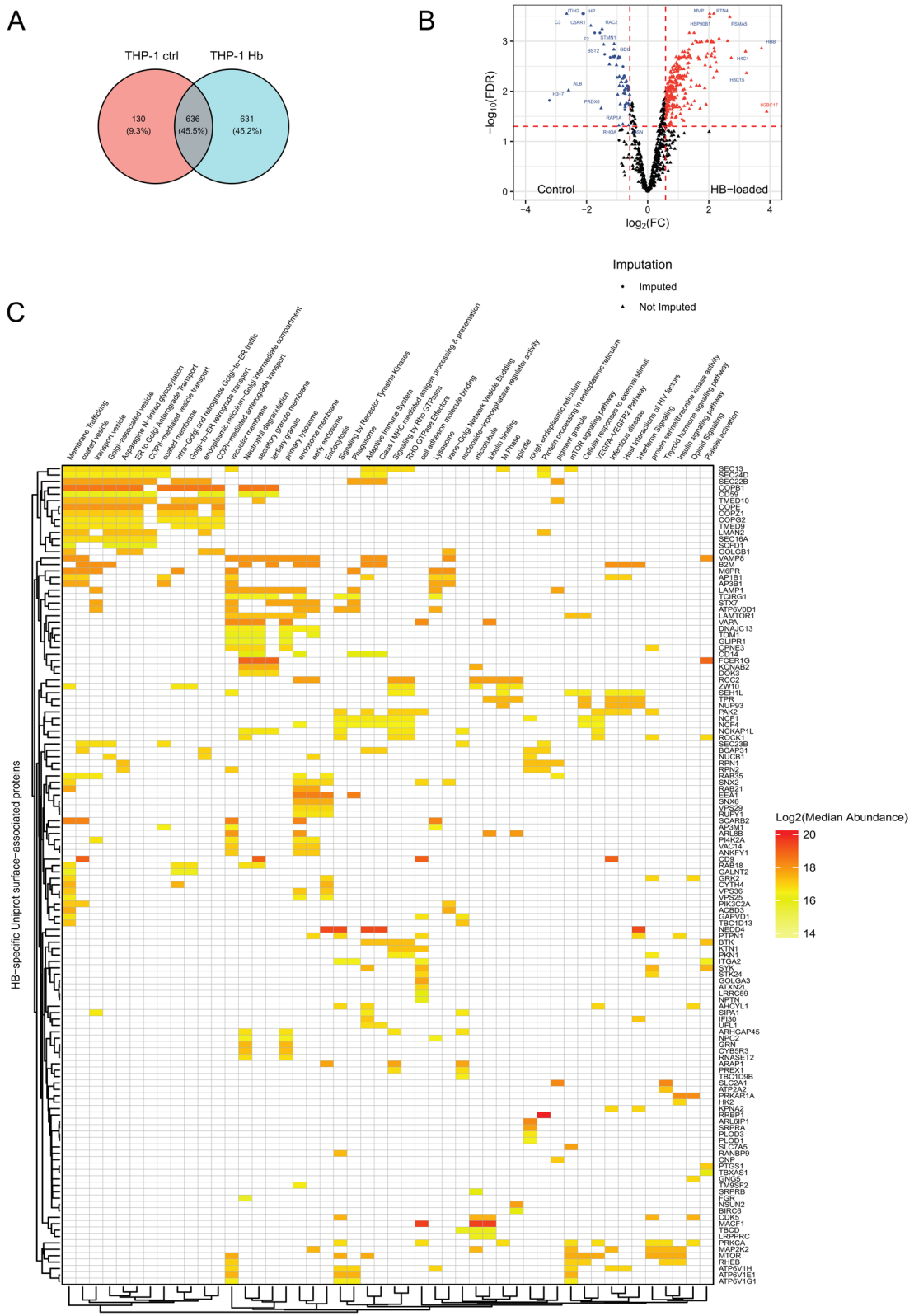

Fig. 4 Proteomic analysis of EV content **A**-**C**. Proteomic analysis of particles collected from 24-h culture of THP-1 macrophages incubated previously with Hb. **A** Venn diagram of proteins detected across experimental groups. **B** Differential expression analysis of protein content of EVs from Hb-treated THP-1 macrophages and control cells. **C** Enrichment map of overrepresented pathways of Uniprot membrane-associated proteins only detected in EVs released by Hb-treated THP-1 macrophages

Table 1 List of questions addressed throughout the manuscript, along with corresponding counterarguments

Tested hypothesis	Arguments against
Is Hb taken up by all macrophages?	Not all macrophages have membrane expression of CD163
Is Hb uptake independent of haptoglobin?	Haptoglobin was shown to be necessary for Hb upake by macrophages
Could Hb be transferred from macrophages to cancer cells?	No earlier observations of this process
Is Hb transferred from macrophages by EV?	Why cytoplasmic Hb would be secreted from macrophages?
Could Hb transfer from macrophages be translated into drug delivery?	Challenge of effective dose delivery in combination with Hb degradation by macrophages

characteristic of secretion and COPI-dependent intracellular vesicle transport (Table 1).

Cytotoxic efficacy of Hb-MMAE-loaded macrophages

To investigate whether the phenomenon of Hb transfer could be exploited as a cancer therapy, we generated a cytotoxic Hb conjugate. Hb was conjugated with monomethyl auristatin E (MMAE) linked by a lysosomally cleavable dipeptide valine-citrulline (vc) fragment. This moiety binds to thiol groups present on cysteines of Hb beta subunits. Mass spectra confirmed that both alpha and beta subunits were successfully conjugated with MMAE (Figure S12A). The beta subunit was slightly more susceptible to conjugation, leaving no free (unconjugated) fraction and attaching up to 3 molecules of MMAE per subunit (up to 2 molecules in the alpha subunit, for comparison). The conjugation efficiency was calculated from the UV–Vis spectrum, presented as the drug-to-protein ratio was 2.3. Native-PAGE showed no degradation of Hb after conjugation (Figure S12B). Next, BMDM were loaded with increasing concentrations (7–500 μg ml^{-1}) of Hb-MMAE, and co-cultured with EMT6 cancer cells for 48 h or 72 h. Already at 48 h of co-culture with BMDM-Hb-MMAE a very high cytotoxicity towards EMT6 was observed (Fig. 5A). Cytotoxicity diminished with decreasing concentrations of Hb-MMAE used for BMDM loading (Fig. 5A). Loading with Hb-MMAE also decreased the viability of co-cultured BMDM, a dose effect was very clear and there was almost no difference between 48 h or 72 h (Figure S12C). Also, human macrophages (THP-1) loaded with Hb-MMAE (1 mg ml^{-1}) showed very robust cytotoxicity for co-cultured human MDA-MB-231 and SKOV-3 cancer cells (Fig. 5B-C). The equivalent concentration of unconjugated Hb had only a transient inhibitory effect on viability of MDA-MB-231 cells at 48 h, and no effect on SKOV-3 cells. In contrast to BMDM, viability of THP-1 cells was not significantly decreased by Hb-MMAE or Hb loading (1 mg ml^{-1}) in both coculture conditions (Figure S12D-E). Using primary hMDM from two different donors and loading with a moderate concentration of Hb-MMAE (0.1 mg ml^{-1}), a very robust and repeatable cytotoxicity effect was observed even at E:T ratio of 0.125:1 (Fig. 5D-E). The numbers of hMDM recovered at the end of the experiment reflected the numbers seeded (Figure S12F-G). Moreover, we found that macrophages loaded with Hb-MMAE increase expression of CD86 (Figure S12H) and do not increase CD206 (Figure S12I) expression on their surface, suggesting acquiring of M1-like phenotype. All these results indicate that macrophages could be used as cellular carriers of cytotoxic conjugates of Hb.

Discussion

Canonically, cell-free Hb is bound to the plasma protein Hp and scavenged by the CD163 receptor on monocytes/macrophages [15]. Following endocytosis by macrophages, Hb is degraded in lysosomes to heme and globin, which is cleaved to amino acids. Heme is converted by the cytosolic enzyme heme oxygenase-1 (HO-1) to antioxidant and anti-inflammatory metabolites: biliverdin, CO, and ferrous iron [14, 16, 29]. Rapid clearance and degradation of Hb are crucial to prevent cellular damage and inflammation leading to various pathologies, that are caused by the oxidative properties of heme [29, 30]. In this study, we showed, for the first time, that Hb can be taken up by macrophages independently of Hp/CD163 and we described a new, alternative pathway of Hb processing in macrophages, namely its transfer to neighboring cells, involving the secretion of EVs.

We have demonstrated that Hp and CD163 are not required for Hb uptake as shown by several different approaches. First, in all experiments we incubated macrophages with Hb in a medium without serum (a potential source of Hp), and the addition of serum or pure Hp generally did not increase Hb uptake. Second, some of the investigated macrophages that took up Hb did not express CD163 mRNA, or expression was low. Furthermore, in the case of macrophages expressing CD163, both $CD163^{+}$ and $CD163^{-}$ populations of macrophages took up Hb. The independence of Hp-Hb complex formation for Hb uptake by CD163 was first shown by Schaer et al. [30] They also showed that $CD163^{-}$ cells do not take up Hb [30], although it was concluded based on an experiment performed on CD163-transduced HEK293,

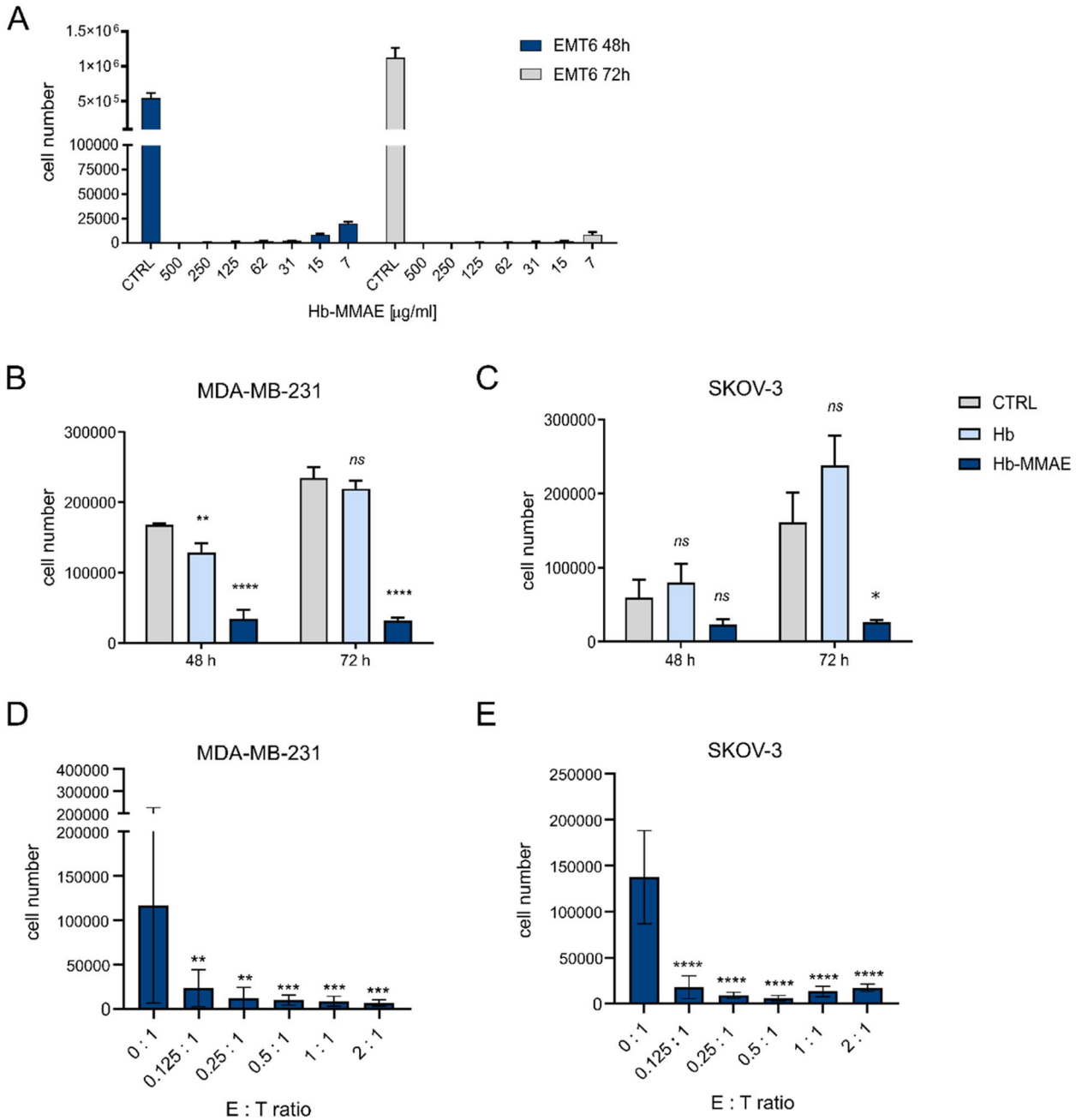

Fig. 5 Cytotoxic effect of macrophages loaded with Hb-MMAE conjugate. **A** Cell number of EMT6 cancer cells co-cultured with BMDM incubated previously with indicated concentrations of Hb-MMAE. Cell number of MDA-MB-231 (**B**.) or SKOV-3 (**C**.) cancer cells co-cultured with THP-1 incubated previously with 1 mg/ml^{-1} of Hb or Hb-MMAE. Cell number of MDA-MB-231 (**D**.) or SKOV-3 (**E**.) cancer cells co-cultured for 48 h at indicated cell ratio with hMDM incubated previously with 0.1 mg ml^{-1} of Hb-MMAE. *$P < 0.05$, ** $P < 0.01$, ***$P < 0.001$, ****$P < 0.0001$. Data are presented as the mean ± SD

not on macrophages, which unlike HEK293, are professional phagocytic cells capable of all types of endocytosis. Moreover, in the study by Schaer et al. CD163 expression on macrophages was shown as mean fluorescence, and is therefore not comparable to our results, which indicate that only a fraction of hMDM express CD163. CD163$^+$ macrophages took up Hb more efficiently than CD163$^-$ macrophages, but CD163$^-$ made up most of the population responsible for Hb uptake. The uptake of Hb by macrophages in our experiments may differ from the

canonical and more physiological situation, due to the Hb concentration used in the experiments. Physiologically, Hp saturation occurs when Hb is 0.5–1.5 mg ml^{-1}. [41] Schaer et al. showed that the presence of Hp improves Hb uptake by macrophages at low Hb concentrations (1 µg ml^{-1} and 10 µg ml^{-1}), but not at Hb concentrations of 100 µg ml^{-1} and higher [30]. In our experiments we did not see such a correlation, Hp increased Hb uptake by macrophages derived from certain donors, but it was not ubiquitous. Nevertheless, we can conclude that the Hb uptake independent of Hp/CD163 may represent a complementary mechanism to canonical Hb clearance, which may be of great importance during massive hemolysis or at sites of injury. The phenomenon of Hb release from macrophages may occur under some non-physiological conditions as the concentration of Hb used in the experiments (0.1 mg ml^{-1}) refers to concentrations of free Hb observed during hemolysis, for example in sickle cell disease (0.01–0.41 mg ml^{-1}), or paroxysmal nocturnal hemoglobinuria (0.5–2 mg ml^{-1} and even 10 mg ml^{-1} during crisis) [42]. Extracorporeal membrane oxygenation (ECMO) therapy causes hemolysis, which can be defined as mild (< 0.5 mg ml^{-1}), moderate (0.5–1.0 mg ml^{-1}), or severe (> 1.0 mg ml^{-1}) depending on the free Hb concentration [43]. Free Hb concentrations of 10–20 mg ml^{-1} have been reported in critically ill patients [44]. In humans, unbound Hb has a lower affinity for the CD163 receptor than the Hb-Hp complex [30]. In contrast to humans, Hp does not promote binding to the CD163 receptor in mice [13], but on the other hand, Hp deficiency in mice increases tissue damage after hemolysis [45]. In addition, CD163-deficient mice have only slightly delayed clearance of Hb [13] and have temporally smaller lesions early after intracerebral hemorrhage [46], suggesting the existence of Hb detoxification mechanisms other than Hp/CD163. An example of such a mechanism is the binding of Hb by soluble CD163 and IgG (Hb-sCD163-IgG) and subsequent uptake of complexes by macrophages and endothelial cells through FcγR [47]. Other known receptors for Hb are F1-ATPase on hepatocytes [48], megalin and cubulin in renal proximal tubules [49]. It is very likely that macrophages use another receptor for Hb uptake, e.g. a scavenger receptor other than CD163, and that they use multiple mechanisms simultaneously. It is worth mentioning, that differences in the mechanisms of Hb detoxification between humans and mice require caution when extrapolating the results of Hb studies from mouse models to humans [50].

All studied macrophages (primary cells and cell lines, human and murine) were shown to be able to transfer Hb to neighboring cells, indicating that the observed process can be defined as a common phenomenon. We have described a more detailed transfer from macrophages to cancer cells, but this route is not unique as Hb is transferred to non-cancer cells as well. In the present study, Hb transfer is protein specific, as albumin, which is also readily taken up by macrophages, is not transferred to cancer cells under the same conditions as Hb. Using flow cytometry, we observed a rapid and efficient transfer of Hb from macrophages to neighboring cells. We further confirmed this observation by microscopy and FCS. Using the second approach, we found the presence of monomers, dimers, and tetramers of Hb in the cytoplasm of recipient MDA-MB-231 cells, but the tetramer was a dominant form of Hb. FCS allows us to distinguish protein-fluorochrome conjugates from pure fluorochrome based on its size, so we are confident of protein transfer.

Although Hb loading was performed at high concentrations in most experiments, its transfer also occurs at ~ 100 × lower concentrations, as shown by FCS analysis. We have shown the transfer of a specific protein, however, but we have not excluded the simultaneous transfer of other proteins within vesicles, as vesicle transfer allows the transfer of several proteins [51].

Due to the unconventional nature of Hb transfer, we investigated its mechanism and we found that Hb is mainly transferred via extracellular vesicles. First, we observed Hb binding to structures resembling intracellular vesicles in recipient cells using FCS. Second, we demonstrated the transfer of Hb via a conditioned medium, suggesting that Hb is released from macrophages and then taken up by recipient cells. Finally, we isolated EVs from a conditioned medium collected from macrophages previously incubated with Hb and found that approximately 30% of EVs released from macrophages contained fluorescently labelled Hb, and that EVs administered to recipient cells were efficiently taken up.

Given the presence of iron in the Hb molecule, the fact that iron is recycled in the body and that macrophages play a key role in this process, we propose that Hb release and transfer may be involved in maintaining iron homeostasis. Iron is mainly exported from cells via ferroportin, but the release of ferritin or heme may be alternative routes [52–54]. Macrophages are the major source of ferritin and ferritin release is increased after erythrophagocytosis or iron administration [55, 56]. Ferritin is released in exosomes and by the nonclassical secretory-autophagy route [57]. Similarly, Hb is released from macrophages into extracellular vesicles. Ferritin release, like Hb release, is not fully understood. However, ferritin secretion appears to be important for local iron redistribution, particularly between cells specialized in iron acquisition (macrophages), iron storage (hepatocytes), and iron consumption (erythroid precursors) [55], as ferritin is directly transferred from macrophages to

erythroid precursors under low transferrin conditions [58]. In addition, ferritin released from macrophages is taken up by hepatocytes [59]. Notably, ferritin transfer occurs in the brain, where microglia secrete ferritin as an essential source of iron for oligodendrocytes [60]. and oligodendrocytes release ferritin as free protein and in extracellular vesicles, which serves as a neuroprotective mechanism [61]. On the other hand, the release of iron-containing Hb may protect macrophages from Hb/iron/heme overload and ferroptosis, and cell death resulting from lipid peroxidation caused by generated reactive oxygen species [62]. The secretion of Hb into EVs may also reflect the state of macrophages, as the quantity and composition of EVs released from Hb-treated macrophages differed from control EVs according to the results of proteomic analysis. It has been shown that stressed cells or cells undergoing inflammation/infection alter the protein profile of EVs [63–65]. Similar to our results, the abundance of proteins related to transcription, translation and histones was previously observed in EVs released from cells exposed to LPS [66, 67]. It can be speculated that the composition of EVs may serve as a danger signal to neighboring cells.

We exploited the process of Hb transfer as a cell-based anticancer drug delivery tool. First, we developed a conjugate of Hb and the anticancer drug MMAE that was loaded into macrophages. Such macrophages effectively kill cancer cells when co-cultured. What interesting, such macrophages acquired an M1-like phenotype, which can be beneficial owing to the antitumor activity of M1 macrophages. The system presented here is completely novel, but each component has been previously studied in the context of drug delivery. Macrophages have emerged as cell-based vehicles for drug delivery due to their migratory properties and phagocytic nature, which allows them to internalize a large amount of cargo [1]. Various cargos have been studied in the context of macrophage delivery, including gold nanoshells for photothermal treatment of glioma, oncolytic viruses targeting prostate cancer, paclitaxel-loaded nanoparticles, melanoma-specific therapeutics, nanoparticle-encapsulated PLX4032, and doxorubicin [68–72]. The therapeutic potential of EVs is also being extensively investigated due to their role in intercellular communication, low immunogenicity and ability to be engineered [73]. EVs-based therapies exploit the innate biological activity of EVs, as in regenerative medicine of the liver or heart [74, 75]. In addition, EVs are exogenously loaded with various molecules including cytostatic drugs, miRNA, siRNA, and enzymes [76]. An especially interesting example involves erythrocyte-derived EVs, which were used to target macrophages in atherosclerotic lesions in mice [77]. Like other iron-binding proteins, Hb was investigated for drug delivery [78]. Hb has been conjugated to ribavirin for hepatitis C, to dichloroacetic acid (DCA), and to floxuridine for anticancer therapy [79–81]. In addition to conjugation, a drug can be entrapped in a heme pocket as has been shown for paclitaxel [82]. Moreover, Hb and doxorubicin-loaded liposomes with Hb on the surface have been tested in the therapy of hypoxic tumors [83]. Of note, Hb conjugate with floxuridine (TBI 302) is being tested in clinical trial in patients with hepatocellular carcinoma (NCT03908840). MMAE is a very potent antimitotic agent, an inhibitor of tubulin polymerization. Since its potency is at the level of nanomoles, which leads to high toxicity, it is used only in the conjugated form in antibody–drug conjugates (ADCs) [84, 85]. Most of the MMAE-containing ADCs have a cathepsin B-cleavable linker (valine-citrulline [vc]) the same that we used when conjugating MMAE to Hb [86]. vcMMAE-ADCs showed better *iv vitro* efficacy and lower in vivo toxicity than hydrazine linkers [87]. However, ADC with MMAE linked by ionized cysteine was shown to have better safety, stability and lower bystander effect [84]. Interestingly, in addition to cytotoxic activity, MMAE has been shown to sensitize cells to radiation-mediated cell damage, resulting in anti-tumor immune response and memory-improving immune checkpoint therapy, which is an added value [88]. In our approach, Hb-MMAE is shielded by both mouse and human macrophages that do not degrade it and effectively transfer it to kill cancer cells in vitro.

Conclusions

Taken together, our results indicate that macrophages can take up Hb independently of Hp/CD163. Instead of being degraded, a significant proportion of Hb is released from macrophages, mainly in extracellular vesicles. The released Hb is then taken up by cells in the vicinity of the macrophages. The process described has the potential to be used as a cellular drug therapy.

Supplementary Information

The online version contains supplementary material available at https://doi.org/10.1186/s12964-024-01929-8.

Additional file 1: Document S1. Figures S1–S12 and Tables S1, S2 and S3.

Acknowledgements

The authors thank for advice to Michael Weller from Laboratory of Molecular Neuro-Oncology, Department of Neurology, Clinical Neuroscience Center, University Hospital and University of Zurich, Switzerland, and Marta Miaczynska from Laboratory of Cell Biology, International Institute of Molecular and Cell Biology, Warsaw, Poland. Schematics were generated with BioRender.com.

Authors' contributions

A.Braniewska: conceptualization, planning of experimental set up, execution of majority of experiments, data analysis, manuscript writing. M.S., Z.S., D.S. and M. Bialasek: cell-culture and flow cytometry experiments. M.D. and M.C-K.:

analysis of EVs. I.M. D.K.: production of the Hb conjugate. M.Bühler and T.W.: proteomic analysis of EVs. A.K. and K.K.: fluorescence correlation spectroscopy. J.W. and M.Komorowski: microscopy. L.C. radiolabeling experiment. A.Boffi and M.Krol: conception of the project and manuscript editing. T.P.R.: conception and supervision of the project, funding, manuscript editing. All authors contributed to manuscript preparation and editing.

Funding
This work was supported by the TEAM TECH /2016–1/8 grant from Foundation for Polish Science (to T.P.R.), A.K. and K.K. were supported by the DIALOG-0188/DLG/2018/10 project. A.Boffi was supported by the "NextGenerationEU" DD. 3175/2021 E DD.3138/2021 CN_3: National Center for Gene Therapy and Drugs based on RNA Technology, code n CN 00000041. The contribution of LC was realized within the National Science Centre, Grant: 2019/35/N/ST4/01987.

Data availability
No datasets were generated or analysed during the current study.

Declarations

Ethics approval and consent to participate
Human primary monocytes were isolated from buffy coats of healthy donors obtained from the Regional Blood Center in Warsaw, Poland, with the knowledge of the Bioethics Committee at the Central Clinical Hospital of the Ministry of Interior and Administration in Warsaw (approved on12/10/2022).

Competing interests
A.Boffi, M.Krol, and T.P.R. are founders and shareholders of Cellis. M.Krol, and T.P.R are members of the board of Cellis. A.Braniewska, M.S., Z.S., IM, A.Boffi, M.Krol, and T.P.R. are authors of patent applications and/or registrations related to this work. A.Braniewska, M.S., Z.S., I.M., D.K., D.S., M.B., L.C., M.Krol, and T.P.R. were or are employees of Cellis. Cellis is a company pursuing the commercial development of related technology.

Received: 20 September 2024 Accepted: 5 November 2024
Published online: 27 November 2024

References

1. Si J, Shao S, Shen Y, Wang K. Macrophages as active nanocarriers for targeted early and adjuvant cancer chemotherapy. Small. 2016;12(37):5108–19.
2. Xiang J, Zhao R, Wang B, Sun X, Guo X, Tan S, et al. Advanced nano-carriers for anti-tumor drug loading. Front Oncol. 2021;11:1–7.
3. Agrahari V, Agrahari V, Mitra AK. Next generation drug delivery: circulatory cells-mediated nanotherapeutic approaches. Expert Opin Drug Deliv. 2017;14(3):285–9.
4. Locati M, Curtale G, Mantovani A. Diversity, mechanisms, and significance of macrophage plasticity. Annu Rev Pathol Mech Dis. 2020;15:123–47.
5. Atri C, Guerfali FZ, Laouini D. Role of human macrophage polarization in inflammation during infectious diseases. Int J Mol Sci. 2018;19(6):1801.
6. Wculek SK, Dunphy G, Heras-Murillo I, Mastrangelo A, Sancho D. Metabolism of tissue macrophages in homeostasis and pathology. Cell Mol Immunol. 2022;19(3):384–408.
7. Klei TRL, Meinderts SM, van den Berg TK, van Bruggen R. From the cradle to the grave: the role of macrophages in erythropoiesis and erythrophagocytosis. Front Immunol. 2017;8:73.
8. Shaeffer JR, McDonald MJ, Turci SM, Dinda DM, Bunn HF. Dimer-monomer dissociation of human hemoglobin A. J Biol Chem. 1984;259(23):14544–7.
9. Nagel RL, Gibson QH. The binding of hemoglobin to haptoglobin and its relation to subunit dissociation of hemoglobin. J Biol Chem. 1971;246(1):69–73.
10. Hall JE, Guyton AC. Guyton and Hall Textbook of Medical Physiology. Philadelphia: Saunders Elsevier; 2011.
11. Jeney V, Balla J, Yachie A, Varga Z, Vercellotti GM, Eaton JW, et al. Pro-oxidant and cytotoxic effects of circulating heme. Blood. 2002;100(3):879–87.
12. Rother RP, Bell L, Hillmen P. The clinical sequelae of intravascular hemolysis and extracellular plasma hemoglobin. JAMA. 2015;293(13):1653–62.
13. Etzerodt A, Kjolby M, Nielsen MJ, Maniecki M, Svendsen P, Moestrup SK. Plasma clearance of hemoglobin and haptoglobin in mice and effect of CD163 gene targeting disruption. Antioxid Redox Signal. 2013;18(17):2254–63.
14. Thomsen JH, Etzerodt A, Svendsen P, Moestrup SK. The haptoglobin-CD163-heme oxygenase-1 pathway for hemoglobin scavenging. Oxid Med Cell Longev. 2013;2013:523652.
15. Kristiansen M, Graversen JH, Jacobsen C, Sonne O, Hoffman HJ, Law SK, et al. Identification of the haemoglobin scavenger receptor. Nature. 2001;409(6817):198–201.
16. Ehrenreich BA. Fate of hemoglobin Pincytosed by macrophages in vitro. J Cell Biol. 1968;38(1):244–8.
17. Schaer DJ, Alayash AI. Clearance and control mechanisms of hemoglobin from cradle to grave. Antioxid Redox Signal. 2010;12(2):181–4.
18. Kalwarczyk T, Kwapiszewska K, Szczepanski K, Sozanski K, Szymanski J, Michalska B, et al. Apparent anomalous diffusion in the cytoplasm of human cells: the effect of probes' polydispersity. J Phys Chem B. 2017;121(42):9831–7.
19. Kwapiszewska K, Kalwarczyk T, Michalska B, Szczepański K, Szymański J, Patalas-Krawczyk P, et al. Determination of oligomerization state of Drp1 protein in living cells at nanomolar concentrations. Sci Rep. 2019;9(1):1–9.
20. Kwapiszewska K, Szczepański K, Kalwarczyk T, Michalska B, Patalas-Krawczyk P, Szymański J, et al. Nanoscale viscosity of cytoplasm is conserved in human cell lines. J Phys Chem Lett. 2020;11(16):6914–20.
21. Karpińska A, Pilz M, Buczkowska J, Żuk PJ, Kucharska K, Magiera G, et al. Quantitative analysis of biochemical processes in living cells at a single-molecule level: a case of olaparib–PARP1 (DNA repair protein) interactions. Analyst. 2021;146(23):7131–43.
22. Ludwig N, Hong CS, Ludwig S, Azambuja JH, Sharma P, Theodoraki MN, et al. Isolation and analysis of tumor-derived exosomes. Curr Protoc Immunol. 2019;127(1):e91.
23. Dlugolecka M, Szymanski J, Zareba L, Homoncik Z, Domagala-Kulawik J, Polubiec-Kownacka M, et al. Characterization of extracellular vesicles from bronchoalveolar lavage fluid and plasma of patients with lung lesions using fluorescence nanoparticle tracking analysis. Cells. 2021;10(12):3473.
24. Teo GC, Polasky DA, Yu F, Nesvizhskii AI. Fast deisotoping algorithm and its implementation in the MSFragger search engine. J Proteome Res. 2021;20(1):498–505.
25. Gianetto QG, Wieczorek S, Couté Y, Burger T. A peptide-level multiple imputation strategy accounting for the different natures of missing values in proteomics data. bioRxiv. 2020;2020.05.29.122770.
26. Ritchie ME, Phipson B, Wu D, Hu Y, Law CW, Shi W, et al. limma powers differential expression analyses for RNA-sequencing and microarray studies. Nucleic Acids Res. 2015;43(7):e47.
27. Gu Z, Eils R, Schlesner M. Complex heatmaps reveal patterns and correlations in multidimensional genomic data. Bioinformatics. 2016;32(18):2847–9.
28. Schaer CA, Vallelian F, Imhof A, Schoedon G, Schaer DJ. CD163-expressing monocytes constitute an endotoxin-sensitive Hb clearance compartment within the vascular system. J Leukoc Biol. 2007;82(1):106–10.
29. Schaer CA, Schoedon G, Imhof A, Kurrer MO, Schaer DJ. Constitutive endocytosis of CD163 mediates hemoglobin-heme uptake and determines the noninflammatory and protective transcriptional response of macrophages to hemoglobin. Circ Res. 2006;99(9):943–50.
30. Schaer DJ, Schaer CA, Buehler PW, Boykins RA, Schoedon G, Alayash AI, et al. CD163 is the macrophage scavenger receptor for native and chemically modified hemoglobins in the absence of haptoglobin. Blood. 2006;107(1):373–80.
31. Karpinska A, Magiera G, Kwapiszewska K, Hołyst R. Cellular uptake of Bevacizumab in cervical and breast cancer cells revealed by single-molecule spectroscopy. J Phys Chem Lett. 2023;14(5):1272–8.
32. Huang YX, Wu ZJ, Huang BT, Luo M. Pathway and mechanism of pH dependent human hemoglobin tetramer-dimer- monomer dissociations. PLoS One. 2013;8(11):1–9.
33. Rustom A, Saffrich R, Markovic I, Walther P, Gerdes H. Nanotubular highways for intercellular organelle transport. Science. 2004;303(5660):1007–10.

34. De Rooij B, Polak R, Stalpers F, Pieters R, den Boer ML. Tunneling nanotubes facilitate autophagosome transfer in the leukemic niche. Leukemia. 2017;31(7):1651–4.
35. Polak R, De Rooij B, Pieters R, den Boer ML. B-cell precursor acute lymphoblastic leukemia cells use tunneling nanotubes to orchestrate their microenvironment. Blood. 2015;126(21):2404–14.
36. Hase K, Kimura S, Takatsu H, Ohmae M, Kawano S, Kitamura H, et al. M-Sec promotes membrane nanotube formation by interacting with Ral and the exocyst complex. Nat Cell Biol. 2009;11(12):1427–32.
37. Pergu R, Dagar S, Kumar H, Kumar R, Bhattacharya J, Mylavarapu SVS. The chaperone ERp29 is required for tunneling nanotube formation by stabilizing MSec. J Biol Chem. 2019;294(18):7177–93.
38. Kimura S, Yamashita M, Yamakami-Kimura M, Sato Y, Yamagata A, Kobashigawa Y, et al. Distinct roles for the N- and C-terminal regions of M-Sec in plasma membrane deformation during tunneling nanotube formation. Sci Rep. 2016;6:33548.
39. Thayanithy V, O'Hare P, Wong P, Zhao X, Steer CJ, Subramanian S, et al. A transwell assay that excludes exosomes for assessment of tunneling nanotube-mediated intercellular communication. Cell Commun Signal. 2017;15(1):46.
40. Onfelt B, Nedvetzki S, Benninger RK, Purbhoo MA, Sowinski S, Hume AN, et al. Structurally distinct membrane nanotubes between human macrophages support long-distance vesicular traffic or surfing of bacteria. J Immunol. 2006;177(12):8476–83.
41. Langlois MR, Delanghe JR. Biological and clinical significance of haptoglobin polymorphism in humans. Clin Chem. 1996;42(10):1589–600.
42. Misztal T, Tomasiak M. Patofizjologiczne konsekwencje hemolizy. Rola wolnej hemoglobiny [Pathophysiological consequences of hemolysis. Role of cell-free hemoglobin]. Postepy Hig Med Dosw (Online). 2011;65:627–39. Polish.
43. Lou S, MacLaren G, Best D, Delzoppo C, Butt W. Hemolysis in pediatric patients receiving centrifugal-pump extracorporeal membrane oxygenation: prevalence, risk factors, and outcomes. Crit Care Med. 2014;42(5):1213–20.
44. Janz DR, Bastarache JA, Peterson JF, Sills G, Wickersham N, May AK, et al. Association between cell-free hemoglobin, acetaminophen, and mortality in patients with sepsis: an observational study. Crit Care Med. 2013;41(3):784–90.
45. Lim SK, Kim H, Lim SK, bin Ali A, Lim YK, Wang Y, et al. Increased susceptibility in Hp knockout mice during acute hemolysis. Blood. 1998;92(6):1870–7.
46. Leclerc JL, Lampert AS, Loyola Amador C, Schlakman B, Vasilopoulos T, Svendsen P, et al. The absence of the CD163 receptor has distinct temporal influences on intracerebral hemorrhage outcomes. J Cereb Blood Flow Metab. 2018;38(2):262–73.
47. Subramanian K, Du R, Tan NS, Ho B, Ding JL. CD163 and IgG codefend against cytotoxic hemoglobin via autocrine and paracrine mechanisms. J Immunol. 2013;190(10):5267–78.
48. Gburek J, Konopska B, Juszczynska K, Piwowar A, Dziegiel P, Borska S, et al. Hemoglobin - a novel ligand of hepatocyte ectopic F1-ATPase. J Physiol Pharmacol. 2015;66(6):823–30.
49. Gburek J, Verroust PJ, Willnow TE, Fyfe JC, Nowacki W, Jacobsen C, et al. Megalin and cubilin are endocytic receptors involved in renal clearance of hemoglobin. J Am Soc Nephrol. 2002;13(2):423–30.
50. Etzerodt A, Moestrup SK. CD163 and inflammation: biological, diagnostic, and therapeutic aspects. Antioxid Redox Signal. 2013;18(17):2352–63.
51. Kolba MD, Dudka W, Zaręba-Kozioł M, Kominek A, Ronchi P, Turos L, et al. Tunneling nanotube-mediated intercellular vesicle and protein transfer in the stroma-provided imatinib resistance in chronic myeloid leukemia cells. Cell Death Dis. 2019;10(11):817.
52. Ganz T. Review macrophages and iron metabolism. Immunity. 2016;44(3):492–504.
53. Cohen LA, Gutierrez L, Weiss A, Leichtmann-Bardoogo Y, Zhang DL, Crooks DR, et al. Serum ferritin is derived primarily from macrophages through a nonclassical secretory pathway. Blood. 2010;116(9):1574–84.
54. Keel SB, Doty RT, Yang Z, Quigley JG, Chen J, Knoblaugh S, et al. A heme export protein is required for red blood cell differentiation and iron homeostasis. Science. 2008;319(5864):825–8.
55. Meyron-Holtz EG, Moshe-Belizowski S, Cohen LA. A possible role for secreted ferritin in tissue iron distribution. J Neural Transm. 2011;118(3):337–47.
56. Yuan XM, Li W, Baird SK, Carlsson M, Melefors Ö. Secretion of ferritin by iron-laden macrophages and influence of lipoproteins. Free Radic Res. 2004;38(10):1133–42.
57. Truman-Rosentsvit M, Berenbaum D, Spektor L, Cohen LA, Belizowsky-Moshe S, Lifshitz L, et al. Ferritin is secreted via 2 distinct nonclassical vesicular pathways. Blood. 2018;131(3):342–52.
58. Leimberg MJ, Prus E, Konijn AM, Fibach E. Macrophages function as a ferritin iron source for cultured human erythroid precursors. J Cell Biochem. 2008;103(4):1211–8.
59. Sibille J-C, Kondo H, Aisen P. Interactions between isolated hepatocytes and kupffer cells in iron metabolism: a possible role for ferritin as an iron carrier protein. Hepatology. 1988;8(2):296–301.
60. Schonberg DL, McTigue DM. Iron is essential for oligodendrocyte genesis following intraspinal macrophage activation. Exp Neurol. 2009;218(1):64–74.
61. Mukherjee C, Kling T. Oligodendrocytes provide antioxidant defense function for neurons by secreting ferritin heavy chain. Cell Metab. 2020;32(2):259–272.e10.
62. Chen X, Yu C, Kang R, Tang D. Iron metabolism in ferroptosis. Front Cell Dev Biol. 2020;8(October):1–14.
63. de Jong OG, Verhaar MC, Chen Y, Vader P, Gremmels H, Posthuma G, et al. Cellular stress conditions are reflected in the protein and RNA content of endothelial cell-derived exosomes. J Extracell Vesicles. 2012;1.
64. Cypryk W, Öhman T, Eskelinen EL, Matikainen S, Nyman TA. Quantitative proteomics of extracellular vesicles released from human monocyte-derived macrophages upon β-glucan stimulation. J Proteome Res. 2014;13(5):2468–77.
65. Dozio V, Sanchez JC. Characterisation of extracellular vesicle-subsets derived from brain endothelial cells and analysis of their protein cargo modulation after TNF exposure. J Extracell Vesicles. 2017;6(1):1–14.
66. Yang Y, Boza-Serrano A, Dunning CJR, Clausen BH, Lambertsen KL, Deierborg T. Inflammation leads to distinct populations of extracellular vesicles from microglia. J Neuroinflammation. 2018;15(1):1–19.
67. Nair RR, Mazza D, Brambilla F, Gorzanelli A, Agresti A, Bianchi ME. LPS-challenged macrophages release microvesicles coated with histones. Front Immunol. 2018;9(JUN):1–15.
68. Baek SK, Makkouk AR, Krasieva T, Sun CH, Madsen SJ, Hirschberg H. Photothermal treatment of glioma; an in vitro study of macrophage-mediated delivery of gold nanoshells. J Neurooncol. 2011;104(2):439–48.
69. Muthana M, Giannoudis A, Scott SD, Fang HY, Coffelt SB, Morrow FJ, et al. Use of macrophages to target therapeutic adenovirus to human prostate tumors. Cancer Res. 2011;71(5):1805–15.
70. Li S, Feng S, Ding L, Liu Y, Zhu Q, Qian Z, et al. Nanomedicine engulfed by macrophages for targeted tumor therapy. Int J Nanomedicine. 2016;11:4107–24.
71. Xie Z, Su Y, Kim GB, Selvi E, Ma C, Aragon-Sanabria V, et al. Immune cell-mediated biodegradable theranostic nanoparticles for melanoma targeting and drug delivery. Small. 2017;13(10):1–10.
72. Guo L, Zhang Y, Yang Z, Peng H, Wei R, Wang C, et al. Tunneling nanotubular expressways for ultrafast and accurate M1 macrophage delivery of anticancer drugs to metastatic ovarian carcinoma. ACS Nano. 2019;13(2):1078–96.
73. Esmaeili A, Alini M, Baghaban Eslaminejad M, Hosseini S. Engineering strategies for customizing extracellular vesicle uptake in a therapeutic context. Stem Cell Res Ther. 2022;13(1):1–16.
74. Lou G, Chen Z, Zheng M, Liu Y. Mesenchymal stem cell-derived exosomes as a new therapeutic strategy for liver diseases. Exp Mol Med. 2017;49(6):e346.
75. Adamiak M, Sahoo S. Exosomes in myocardial repair: advances and challenges in the development of next-generation therapeutics. Mol Ther. 2018;26(7):1635–43.
76. Klyachko NL, Arzt CJ, Li SM, Gololobova OA, Batrakova EV. Extracellular vesicle-based therapeutics: preclinical and clinical investigations. Pharmaceutics. 2020;12(12):1–26.
77. Pham TT, Le AH, Dang CP, Chong SY, Do DV, Peng B, et al. Endocytosis of red blood cell extracellular vesicles by macrophages leads to cytoplasmic heme release and prevents foam cell formation in atherosclerosis. J Extracell Vesicles. 2023;12(8):e12354.
78. Bialasek M, Kubiak M, Gorczak M, Braniewska A, Kucharzewska-Siembieda P, Krol M, et al. Exploiting iron-binding proteins for drug delivery. J Physiol Pharmacol. 2019;70(5).

79. Brookes S, Biessels P, Ng NFL, Woods C, Bell DN, Adamson G. Synthesis and characterization of a hemoglobin-ribavirin conjugate for targeted drug delivery. Bioconjug Chem. 2006;17(2):530–7.
80. Zhang N, Palmer AF. Development of a dichloroacetic acid-hemoglobin conjugate as a potential targeted anti-cancer therapeutic. Biotechnol Bioeng. 2011;108(6):1413–20.
81. Brookes S, Levy G, Seo J, Cutler M, Adamson G, Bell D. A first-in-class therapy for the treatment of advanced stage liver cancer. J Clin Oncol. 2016;34(15_suppl):e14061.
82. Meng Z, Yang X, Hu D, Wang K, Zhi F, Chen X, et al. Replacing heme with paclitaxel to prepare drug-loaded globin nanoassembles for CD163 targeting. J Pharm Sci. 2015;104(3):1045–55.
83. Yang J, Li W, Luo L, Jiang M, Zhu C, Qin B, et al. Hypoxic tumor therapy by hemoglobin mediated drug delivery and reversal of hypoxia-induced chemoresistance. Biomaterials. 2018;182:145–56.
84. Wang Y, Liu L, Fan S, Xiao D, Xie F, Li W, et al. Antibody-drug conjugate using ionized Cys-Linker-MMAE as the potent payload shows optimal therapeutic safety. Cancers (Basel). 2020;12(3):744.
85. Birrer MJ, Moore KN, Betella I, Bates RC. Antibody-drug conjugate-based therapeutics: state of the science. J Natl Cancer Inst. 2019;111(6):538–49.
86. Li C, Zhang C, Li Z, Samineni D, Lu D, Wang B, et al. Clinical pharmacology of vc-MMAE antibody-drug conjugates in cancer patients: learning from eight first-in-human Phase 1 studies. MAbs. 2020;12(1):1699768.
87. Doronina SO, Toki BE, Torgov MY, Mendelsohn BA, Cerveny CG, Chace DF, et al. Development of potent monoclonal antibody auristatin conjugates for cancer therapy. Nat Biotechnol. 2003;21(7):778–84.
88. Hingorani DV, Allevato MM, Camargo MF, Lesperance J, Quraishi MA, Aguilera J, et al. Monomethyl auristatin antibody and peptide drug conjugates for trimodal cancer chemo-radio-immunotherapy. Nat Commun. 2022;13(1):3869.

Publisher's Note